nature

https://doi.org/10.1038/s41586-020-2923-3

Accelerated Article Preview

Mobility network models of COVID-19 explain inequities and inform reopening

Received: 15 June 2020

Accepted: 21 October 2020

Accelerated Article Preview Published online 10 November 2020

Cite this article as: Chang, S. et al. Mobility network models of COVID-19 explain inequities and inform reopening. *Nature* https://doi.org/10.1038/s41586-020-2923-3 (2020).

Serina Chang, Emma Pierson, Pang Wei Koh, Jaline Gerardin, Beth Redbird, David Grusky & Jure Leskovec

Mobility network models of COVID-19 explain inequities and inform reopening

https://doi.org/10.1038/s41586-020-2923-3

Received: 15 June 2020

Accepted: 21 October 2020

Published online: 10 November 2020

Serina Chang[1,9], Emma Pierson[1,2,9], Pang Wei Koh[1,9], Jaline Gerardin[3], Beth Redbird[4,5], David Grusky[6,7] & Jure Leskovec[1,8] ✉

The COVID-19 pandemic dramatically changed human mobility patterns, necessitating epidemiological models which capture the effects of changes in mobility on virus spread[1]. We introduce a metapopulation SEIR model that integrates fine-grained, dynamic mobility networks to simulate the spread of SARS-CoV-2 in 10 of the largest US metropolitan statistical areas. Derived from cell phone data, our mobility networks map the hourly movements of 98 million people from neighborhoods (census block groups, or CBGs) to points of interest (POIs) such as restaurants and religious establishments, connecting 57k CBGs to 553k POIs with 5.4 billion hourly edges. We show that by integrating these networks, a relatively simple SEIR model can accurately fit the real case trajectory, despite substantial changes in population behavior over time. Our model predicts that a small minority of "superspreader" POIs account for a large majority of infections and that restricting maximum occupancy at each POI is more effective than uniformly reducing mobility. Our model also correctly predicts higher infection rates among disadvantaged racial and socioeconomic groups[2–8] solely from differences in mobility: we find that disadvantaged groups have not been able to reduce mobility as sharply, and that the POIs they visit are more crowded and therefore higher-risk. By capturing who is infected at which locations, our model supports detailed analyses that can inform more effective and equitable policy responses to COVID-19.

In response to the COVID-19 crisis, stay-at-home orders were enacted in many countries to reduce contact between individuals and slow the spread of the virus[9]. Since then, public officials have continued to deliberate over when to reopen, which places are safe to return to, and how much activity to allow[10]. Answering these questions requires epidemiological models that can capture the effects of changes in mobility on virus spread. In particular, findings of COVID-19 "super-spreader" events[11–14] motivate models that can reflect the heterogeneous risks of visiting different locations, while well-reported disparities in infection rates[2–8] require models that can explain the disproportionate impact of the virus on disadvantaged groups.

To address these needs, we construct fine-grained dynamic mobility networks from cell phone geolocation data, and use these networks to model the spread of SARS-CoV-2 within 10 of the largest metropolitan statistical areas (referred to below as metro areas) in the United States. These networks map the hourly movements of 98 million people from census block groups (CBGs), which are geographical units that typically contain 600–3,000 people, to specific points of interest (POIs). As shown in Table S1, POIs are non-residential locations that people visit such as restaurants, grocery stores, and religious establishments. On top of each network, we overlay a metapopulation SEIR model that tracks the infection trajectories of each CBG as well as the POIs at which these infections are likely to have occurred. This builds upon prior work that models disease spread using aggregate[15–19], historical[20–22], or synthetic mobility data[23–25]; separately, other work has analyzed mobility data in the context of COVID-19, but without an underlying model of disease spread[26–30].

Combining our epidemiological model with these mobility networks allows us to not only accurately fit observed case counts, but also to conduct detailed analyses that can inform more effective and equitable policy responses to COVID-19. By capturing information about individual POIs (e.g., hourly number of visitors, median visit duration), our model can estimate the impacts of specific reopening strategies, such as only reopening certain POI categories or restricting maximum occupancy at each POI. By modeling movement from CBGs, our model can identify at-risk populations and correctly predict, solely from mobility patterns, that disadvantaged racial and socioeconomic groups face higher rates of infection. Our model thus enables analysis of urgent health disparities; we use it to illuminate two mobility-related mechanisms driving these disparities and to evaluate the disparate impact of reopening on disadvantaged groups.

Mobility network model

We use data from SafeGraph, a company that aggregates anonymized location data from mobile applications, to study mobility patterns from

[1]Department of Computer Science, Stanford University, Stanford, CA, 94305, USA. [2]Microsoft Research, Cambridge, MA, 02142, USA. [3]Department of Preventive Medicine, Northwestern University, Chicago, IL, 60611, USA. [4]Department of Sociology, Northwestern University, Evanston, IL, 60208, USA. [5]Institute for Policy Research, Northwestern University, Evanston, IL, 60208, USA. [6]Department of Sociology, Stanford University, Stanford, CA, 94305, USA. [7]Center on Poverty and Inequality, Stanford University, Stanford, CA, 94305, USA. [8]Chan Zuckerberg Biohub, San Francisco, CA, 94158, USA. [9]These authors contributed equally: Serina Chang, Emma Pierson, Pang Wei Koh. ✉e-mail: jure@cs.stanford.edu

March 1–May 2, 2020. For each metro area, we represent the movement of individuals between CBGs and POIs as a bipartite network with time-varying edges, where the weight of an edge between a CBG and POI represents the number of visitors from that CBG to that POI at a given hour (Figure 1a). SafeGraph also provides the area in square feet of each POI, as well as its North American Industry Classification System (NAICS) category (e.g., fitness center, full-service restaurant) and median visit duration in minutes. We validated the SafeGraph mobility data by comparing to Google mobility data (Figure S1, Tables S2–S3), and used iterative proportional fitting[31] to derive POI-CBG networks from the raw SafeGraph data. Overall, these networks comprise 5.4 billion hourly edges between 56,945 CBGs and 552,758 POIs (ED Table 1).

We overlay a SEIR model on each mobility network[15,20], where each CBG maintains its own susceptible (S), exposed (E), infectious (I), and removed (R) states (Figure 1b). New infections occur at both POIs and CBGs, with the mobility network governing how subpopulations from different CBGs interact as they visit POIs. We use each POI's area, median visit duration, and time-varying density of infectious individuals to determine the POI's hourly infection rate. The model has only three free parameters, which scale (1) transmission rates at POIs, (2) transmission rates at CBGs, and (3) the initial proportion of exposed individuals (ED Table 2); all three parameters remain constant over time. We calibrate a separate model for each metro area using confirmed case counts from *The New York Times* by minimizing root mean square error (RMSE) to daily incident cases[32]. Our model accurately fits observed daily case counts in all 10 metro areas from March 8–May 9, 2020 (Figure 1c,d). Additionally, when only calibrated on case counts up to April 14, the model predicts case counts reasonably well on the held-out time period from April 15–May 9, 2020 (Figure 1c and ED Figure 1a). Our key technical finding is that the dynamic mobility network allows even our relatively simple SEIR model with just three static parameters to accurately fit observed cases, despite changing policies and behaviors during that period.

Mobility reduction and reopening plans

The magnitude of mobility reduction is at least as important as its timing

Mobility in the US dropped sharply in March 2020: e.g., overall POI visits in the Chicago metro area fell by 54.7% between the first week of March and the first week of April 2020. We constructed counterfactual mobility networks by scaling the magnitude of mobility reduction down and by shifting the timeline earlier and later, and applied our model to the counterfactual networks to simulate the resulting infection trajectories. Across metro areas, we found that the magnitude of mobility reduction was at least as important as its timing (Figure 2a, Tables S4–S5): e.g., if the mobility reduction in the Chicago metro area had been only one quarter as large, predicted infections would have increased by 3.3× (95% CI, 2.8-3.8), compared to a 1.5× (95% CI, 1.4–1.6) increase had people begun reducing their mobility one full week later. Furthermore, if no mobility reduction had occurred at all, predicted infections in the Chicago metro area would have increased by a striking 6.2× (95% CI, 5.2–7.1). Our results concord with earlier findings that mobility reductions can dramatically reduce infections[18,19,33,34].

A minority of POIs account for a majority of predicted infections

We next investigated if *how* we reduce mobility—i.e., to which POIs—matters. We computed the number of infections that occurred at each POI in our simulations from March 1–May 2, 2020, and found that a majority of predicted infections occurred at a small fraction of "superspreader" POIs; e.g., in the Chicago metro area, 10% of POIs accounted for 85% (95% CI, 83%–87%) of the predicted infections at POIs (Figure 2b, Figure S10). Certain categories of POIs also contributed far more to infections (e.g., full-service restaurants, hotels), although our model predicted time-dependent variation in how much each category contributed (ED Figure 2). For example, restaurants and fitness centers contributed less to predicted infections over time, likely due to lockdown orders closing these POIs, while grocery stores remained steady or even grew in their contribution, which concords with their status as essential businesses.

Reopening with reduced maximum occupancy

If a minority of POIs produce the majority of infections, then reopening strategies that specifically target high-risk POIs should be especially effective. To test one such strategy, we simulated reopening on May 1, and modeled the effects of reducing maximum occupancy in which the numbers of hourly visits to each POI returned to their "normal" levels from the first week of March but were capped if they exceeded a fraction of the POI's maximum occupancy[35]. Full reopening without reducing maximum occupancy produced a spike in predicted infections: in the Chicago metro area, our models projected that an additional 32% (95% CI, 25%–35%) of the population would be infected by the end of May (Figure 2c). However, reducing maximum occupancy substantially reduced risk without sharply reducing overall mobility: capping at 20% maximum occupancy in the Chicago metro area cut down predicted new infections by more than 80% but only lost 42% of overall visits, and we observed similar trends across other metro areas (ED Figure 3). This highlights the non-linearity of predicted infections as a function of visits: one can achieve a disproportionately large reduction in infections with a small reduction in visits. Furthermore, compared to another reopening strategy that uniformly reduced visits to each POI from their levels in early March, reducing maximum occupancy always resulted in fewer predicted infections for the same number of total visits (Figure 2c and ED Figure 4). This is because reduced maximum occupancy takes advantage of the time-varying visit density within each POI, disproportionately reducing visits to the POI during the most risky high-density periods, but leaving visit counts unchanged during less risky periods. These results support earlier findings that precise interventions, like reducing maximum occupancy, may be more effective than less targeted measures, while incurring substantially lower economic costs[36].

Relative risk of reopening different categories of POIs

Because we found that certain POI categories contributed far more to predicted infections in March (ED Figure 2), we also expected that reopening some POI categories would be riskier than reopening others. To assess this, we simulated reopening each category in turn on May 1 (by returning its mobility patterns to early March levels, as before), while keeping all other POIs at their reduced mobility levels from the end of April. We found large variation in predicted reopening risks: on average across metro areas, full-service restaurants, gyms, hotels, cafes, religious organizations, and limited-service restaurants produced the largest predicted increases in infections when reopened (ED Figure 5d). Reopening full-service restaurants was particularly risky: in the Chicago metro area, we predicted an additional 596k (95% CI, 434k–686k) infections by the end of May, more than triple the next riskiest POI category (Figure 2d). These risks are summed over all POIs in the category, but the relative risks after normalizing by the number of POIs were broadly similar (ED Figure 5c). These categories were predicted to more be dangerous because, in the mobility data, their POIs tended to have higher visit densities and/or visitors stayed there longer (Figures S15–S24).

Demographic disparities in infections

We characterize the differential spread of SARS-CoV-2 along demographic lines by using US Census data to annotate each CBG with its racial composition and median income, then tracking predicted infection rates in CBGs with different demographic compositions: for example, within each metro area, comparing CBGs in the top and bottom deciles for income. We use this approach to study the mobility

mechanisms behind disparities and to quantify how different reopening strategies impact disadvantaged groups.

Predicting disparities from mobility data

Despite only having access to mobility data and no demographic information, our models correctly predicted higher risks of infection among disadvantaged racial and socioeconomic groups[2–8]. Across all metro areas, individuals from CBGs in the bottom decile for income were substantially likelier to have been infected by the end of the simulation, even though all individuals began with equal likelihoods of infection (Figure 3a). This predicted disparity was driven primarily by a few POI categories (e.g., full-service restaurants), which infected far larger proportions of lower-income CBGs than higher-income CBGs (Figure 3c and S2). We similarly found that CBGs with fewer white residents had higher predicted risks of infection, although results were more variable across metro areas (Figure 3b). In SI Discussion, we confirm that the magnitude of the disparities our model predicts are generally consistent with real-world disparities and further explore the large predicted disparities in Philadelphia, which stem from substantial differences in the POIs that are frequented by higher- versus lower-income CBGs. In the analysis below, we discuss two mechanisms producing higher predicted infection rates among lower-income CBGs, and we show in ED Figure 6 and ED Table 4 that similar results hold for racial disparities as well.

Lower-income CBGs saw smaller reductions in mobility

A first mechanism producing disparities was that, across all metro areas, lower-income CBGs did not reduce their mobility as sharply in the first few weeks of March 2020, and had higher mobility than higher-income CBGs for most of March through May (Figure 3d, ED Figure 6). For example, in April, lower-income CBGs in the Chicago metro area had 27% more POI visits per capita than higher-income CBGs. Category-level differences in visit patterns partially explained the infection disparities within each category: e.g., lower-income CBGs made substantially more visits per capita to grocery stores than did higher-income CBGs (Figure S3), and consequently experienced more predicted infections at that category (Figure S2).

POIs visited by lower-income CBGs have higher transmission rates

Differences in visits per capita do not fully explain the infection disparities: for example, Cafes & Snack Bars were visited more frequently by higher-income CBGs in every metro area (Figure S3), but our model predicted that Cafes & Snack Bars infected a larger proportion of lower-income CBGs in the majority of metro areas (Figure S2). We found that even within a POI category, the predicted transmission rates at POIs frequented by lower-income CBGs tended to be higher than the corresponding rates for higher-income CBGs (Figure 3e; ED Table 3), because POIs frequented by lower-income CBGs tended to be smaller and more crowded in the mobility data. As a case study, we examined grocery stores in further detail. In 8 of the 10 metro areas, visitors from lower-income CBGs encountered higher predicted transmission rates at grocery stores than visitors from higher-income CBGs (median transmission rate ratio of 2.19, ED Table 3). Why was one visit to the grocery store predicted to be twice as dangerous for a lower-income individual? SafeGraph data showed that the average grocery store visited by lower-income individuals had 59% more hourly visitors per square foot, and their visitors stayed 17% longer on average (medians across metro areas). These findings highlight how fine-grained differences in mobility patterns—how often people go out and which POIs they go to—can ultimately contribute to dramatic disparities in predicted infection outcomes.

Reopening plans must account for disparate impact

Because disadvantaged groups suffer a larger burden of infection, it is critical to not just consider the overall impact of reopening plans but also their disparate impact on disadvantaged groups specifically. For example, our model predicted that full reopening in the Chicago metro area would result in an additional 39% (95% CI, 31%–42%) of the population of CBGs in the bottom income decile being infected within a month, compared to 32% (95% CI, 25%–35%) of the overall population (Figure 3f; results for all metro areas in ED Figure 3). Similarly, Figure S4 illustrates that reopening individual POI categories tends to have a larger predicted impact on lower-income CBGs. More stringent reopening plans produce smaller absolute disparities in predicted infections—e.g., we predict that reopening at 20% of maximum occupancy in Chicago would result in additional infections for 6% (95% CI, 4%–8%) of the overall population and 10% (95% CI, 7%–13%) of the population in CBGs in the bottom income decile (Figure 3f)—though the relative disparity remains.

Discussion

The mobility dataset we use has limitations: it does not cover all populations, does not contain all POIs, and cannot capture sub-CBG heterogeneity. Our model itself is also parsimonious, and does not include all real-world features relevant to disease transmission. We discuss these limitations in more detail in SI Discussion. However, the predictive accuracy of our model suggests that it broadly captures the relationship between mobility and transmission, and we thus expect our broad conclusions—e.g., that people from lower-income CBGs have higher infection rates in part because they tend to visit denser POIs and because they have not reduced mobility by as much (likely because they cannot as easily work from home[4])—to hold robustly. Our fine-grained network modeling approach naturally extends to other mobility datasets and models which capture more aspects of real-world transmission, and these represent interesting directions for future work.

Our results can guide policymakers seeking to assess competing approaches to reopening. Despite growing concern about racial and socioeconomic disparities in infections and deaths, it has been difficult for policymakers to act on those concerns; they are currently operating without much evidence on the disparate impacts of reopening policies, prompting calls for research that both identifies the causes of observed disparities and suggests policy approaches to mitigate them[5,8,37,38]. Our fine-grained mobility modeling addresses both these needs. Our results suggest that infection disparities are not the unavoidable consequence of factors that are difficult to address in the short term, like differences in preexisting conditions; on the contrary, short-term policy decisions can substantially affect infection outcomes by altering the overall amount of mobility allowed and the types of POIs reopened. Considering the disparate impact of reopening plans may lead policymakers to adopt policies that can drive down infection densities in disadvantaged neighborhoods by supporting, e.g., (1) more stringent caps on POI occupancies, (2) emergency food distribution centers to reduce densities in high-risk stores, (3) free and widely available testing in neighborhoods predicted to be high risk (especially given known disparities in access to tests[2]), (4) improved paid leave policy or income supports that allow essential workers to curtail mobility when sick, and (5) improved workplace infection prevention for essential workers, such as high-quality PPE, good ventilation, and distancing when possible. As reopening policies continue to be debated, it is critical to build tools that can assess the effectiveness and equity of different approaches. We hope that our model, by capturing heterogeneity across POIs, demographic groups, and cities, helps address this need.

Online content

Any methods, additional references, Nature Research reporting summaries, source data, extended data, supplementary information, acknowledgements, peer review information; details of author contributions

and competing interests; and statements of data and code availability are available at https://doi.org/10.1038/s41586-020-2923-3.

1. Buckee, C. O. *et al*. Aggregated mobility data could help fight COVID-19. *Science* **368**, 145–146 (2020).
2. Wilson, C. These Graphs Show How COVID-19 Is Ravaging New York City's Low-Income Neighborhoods. *Time* (2020). Available at https://time.com/5821212/coronavirus-low-income-communities/.
3. Garg, S. *et al*. Hospitalization Rates and Characteristics of Patients Hospitalized with Laboratory-Confirmed Coronavirus Disease 2019 — COVID-NET, 14 States, March 1—30, 2020. (CDC Morbidity and Mortality Weekly Report (MMWR), 2020). Available at https://www.cdc.gov/mmwr/volumes/69/wr/mm6915e3.htm.
4. Reeves, R. V. & Rothwell, J. Class and COVID: How the less affluent face double risks. *The Brookings Institution* (2020). Available at https://www.brookings.edu/blog/up-front/2020/03/27/class-and-covid-how-the-less-affluent-face-double-risks/.
5. Pareek, M. *et al*. Ethnicity and COVID-19: an urgent public health research priority. *The Lancet* **395**, 1421–1422 (2020).
6. van Dorn, A., Cooney, R. E. & Sabin, M. L. COVID-19 exacerbating inequalities in the US. *The Lancet* **395**, 1243–1244 (2020).
7. Yancy, C. W. COVID-19 and African Americans. *JAMA* **323**, 1891–1892 (2020).
8. Chowkwanyun, M. & Reed Jr, A. L. Racial Health Disparities and Covid-19—Caution and Context. *New England Journal of Medicine* **383**, 201–203 (2020).
9. Flaxman, S. *et al*. Estimating the effects of non-pharmaceutical interventions on COVID-19 in Europe. *Nature* **584**, 257–261 (2020).
10. Rojas, R. & Delkic, M. As States Reopen, Governors Balance Existing Risks With New Ones. *The New York Times* (2020). Available at https://www.nytimes.com/2020/05/17/us/coronavirus-states-reopen.html.
11. Endo, A. *et al*. Estimating the overdispersion in COVID-19 transmission using outbreak sizes outside China. *Wellcome Open Research* **5** (2020).
12. Adam, D. C. *et al*. Clustering and superspreading potential of SARS-CoV-2 infections in Hong Kong. *Nature Medicine* (2020).
13. Park, S. Y. *et al*. Coronavirus Disease Outbreak in Call Center, South Korea. *Emerging Infectious Diseases* **26**, (2020).
14. Bi, Q. *et al*. Epidemiology and transmission of COVID-19 in 391 cases and 1286 of their close contacts in Shenzhen, China: a retrospective cohort study. *The Lancet Infectious Diseases* **20**, 911–919 (2020).
15. Chinazzi, M. *et al*. The effect of travel restrictions on the spread of the 2019 novel coronavirus (COVID-19) outbreak. *Science* **368**, 395–400 (2020).
16. Jia, J. S. *et al*. Population flow drives spatio-temporal distribution of COVID-19 in China. *Nature* **582**, 389–394 (2020).
17. Pei, S., Kandula, S. & Shaman, J. Differential Effects of Intervention Timing on COVID-19 Spread in the United States. *medRxiv* (2020). Available at https://doi.org/10.1101/2020.05.15.20103655.
18. Lai, S. *et al*. Effect of non-pharmaceutical interventions to contain COVID-19 in China. *Nature* **585**, 410–413 (2020).
19. Badr, H. *et al*. Association between mobility patterns and COVID-19 transmission in the USA: a mathematical modelling study. *The Lancet Infectious Diseases* (2020).
20. Li, R. *et al*. Substantial undocumented infection facilitates the rapid dissemination of novel coronavirus (SARS-CoV2). *Science* **368**, 489–493 (2020).
21. Pei, S. & Shaman, J. Initial Simulation of SARS-CoV2 Spread and Intervention Effects in the Continental US. *medRxiv* (2020). Available at https://doi.org/10.1101/2020.03.21.20040303.
22. Aleta, A. *et al*. Modeling the impact of social distancing, testing, contact tracing and household quarantine on second-wave scenarios of the COVID-19 epidemic. *medRxiv* (2020). Available at https://doi.org/10.1101/2020.05.06.20092841.
23. Duque, D. *et al*. COVID-19: How to Relax Social Distancing If You Must. *medRxiv* (2020). Available at https://doi.org/10.1101/2020.04.29.20085134.
24. Block, P. *et al*. Social network-based distancing strategies to flatten the COVID-19 curve in a post-lockdown world. *Nature Human Behaviour* **4**, 588–596 (2020).
25. Karin, O. *et al*. Adaptive cyclic exit strategies from lockdown to suppress COVID-19 and allow economic activity. *medRxiv* (2020). Available at https://doi.org/10.1101/2020.04.04.20053579.
26. Gao, S. *et al*. Mapping county-level mobility pattern changes in the United States in response to COVID-19. *SIGSPATIAL Special* **12**, 16–26 (2020).
27. Klein, B. *et al*. Assessing changes in commuting and individual mobility in major metropolitan areas in the United States during the COVID-19 outbreak (2020). Available at networkscienceinstitute.org/publications/assessing-changes-in-commuting-and-individual-mobility-in-major-metropolitan-areas-in-the-united-states-during-the-covid-19-outbreak.
28. Benzell, S. G., Collis, A. & Nicolaides, C. Rationing social contact during the COVID-19 pandemic: Transmission risk and social benefits of US locations. *Proceedings of the National Academy of Sciences* **17**, 14642–14644 (2020).
29. Baicker, K. *et al*. Is It Safer to Visit a Coffee Shop or a Gym? *The New York Times* (2020). Available at https://nytimes.com/interactive/2020/05/06/opinion/coronavirus-us-reopen.html.
30. Hsiang, S. *et al*. The effect of large-scale anti-contagion policies on the coronavirus (COVID-19) pandemic. *Nature* **584**, 262–267 (2020).
31. Deming, W. E. & Stephan, F. F. On a least squares adjustment of a sampled frequency table when the expected marginal totals are known. *The Annals of Mathematical Statistics* **11**, 427–444 (1940).
32. The New York Times. Coronavirus (Covid-19) Data in the United States (2020). Available at https://github.com/nytimes/covid-19-data.
33. Tian, H. *et al*. An investigation of transmission control measures during the first 50 days of the COVID-19 epidemic in China. *Science* **368**, 638–642 (2020).
34. Watts, D. J. *et al*. Multiscale, resurgent epidemics in a hierarchical metapopulation model. *Proceedings of the National Academy of Sciences* **102**, 11157–11162 (2020).
35. California Department of Public Health. COVID-19 Industry Guidance: Retail (2020). Available at https://covid19.ca.gov/pdf/guidance-retail.pdf.
36. Birge, J., Candogan, O., & Feng, Y. Controlling Epidemic Spread: Reducing Economic Losses with Targeted Closures (2020). Available at https://bfi.uchicago.edu/wp-content/uploads/BFI_WP_202057-1.pdf.
37. Webb Hooper, M., Nápoles, A. M., & Pérez-Stable, E. J. COVID-19 and Racial/Ethnic Disparities. *JAMA* **323**, 2466–2467 (2020).
38. Laurencin, C. T. & McClinton, A. The COVID-19 Pandemic: a Call to Action to Identify and Address Racial and Ethnic Disparities. *Journal of Racial and Ethnic Health Disparities* **7**, 398–402 (2020).

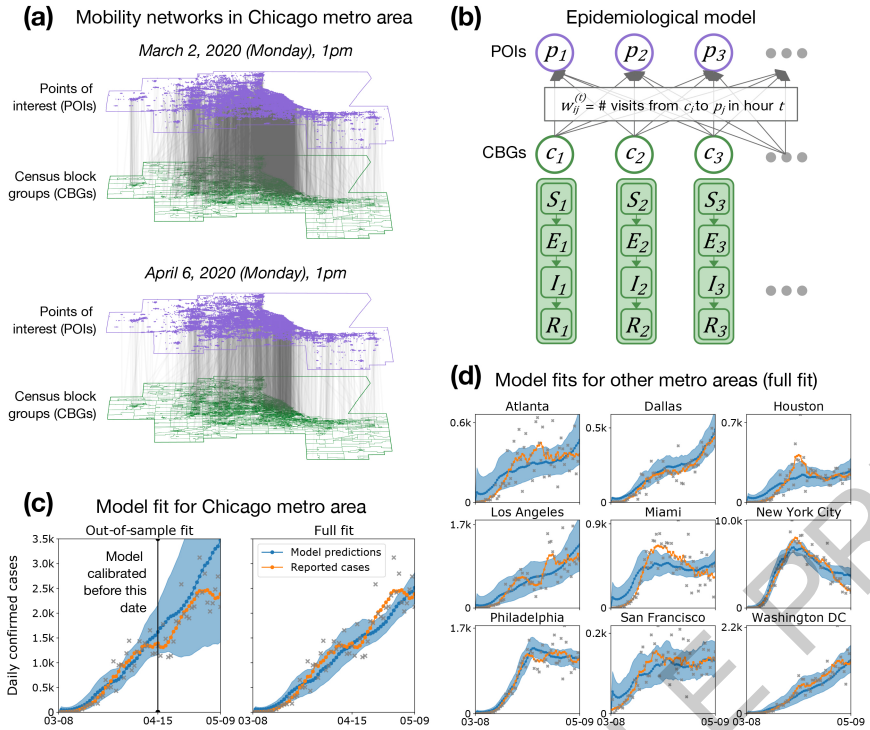

Figure 1 | Model description and fit. (a) The mobility network captures hourly visits from each census block group (CBG) to each point of interest (POI). The vertical lines indicate that most visits are between nearby POIs and CBGs. Visits dropped dramatically from March (top) to April (bottom), as indicated by the lower density of grey lines. **(b)** We overlaid a disease spread model on the mobility network, with each CBG having its own set of SEIR compartments. New infections occur at both POIs and CBGs, with the mobility network governing how subpopulations from different CBGs interact as they visit POIs. **(c)** Left: To test out-of-sample prediction, we calibrated the model on data before April 15, 2020 (vertical black line). Even though its parameters remain fixed over time, the model accurately predicts the case trajectory in the Chicago metro area after April 15 by using mobility data (RMSE on daily cases = 406 for date range April 15–May 9). Right: Model fit further improved when we calibrated the model on the full range of data (RMSE on daily cases = 387 for date range April 15–May 9). **(d)** We fit separate models to 10 of the largest US metropolitan statistical areas, modeling a total population of 98 million people; here, we show full model fits, as in (c)-Right. In (c) and (d), the blue line represents model predictions and grey x's represent the daily reported cases; since they tend to have great variability, we also show the smoothed weekly average (orange line). Shaded regions denote 2.5th and 97.5th percentiles across parameter sets and stochastic realizations. Across metro areas, we sample 97 parameter sets, with 30 stochastic realizations each (N = 2,910); see Table S6 for the number of sets per metro area.

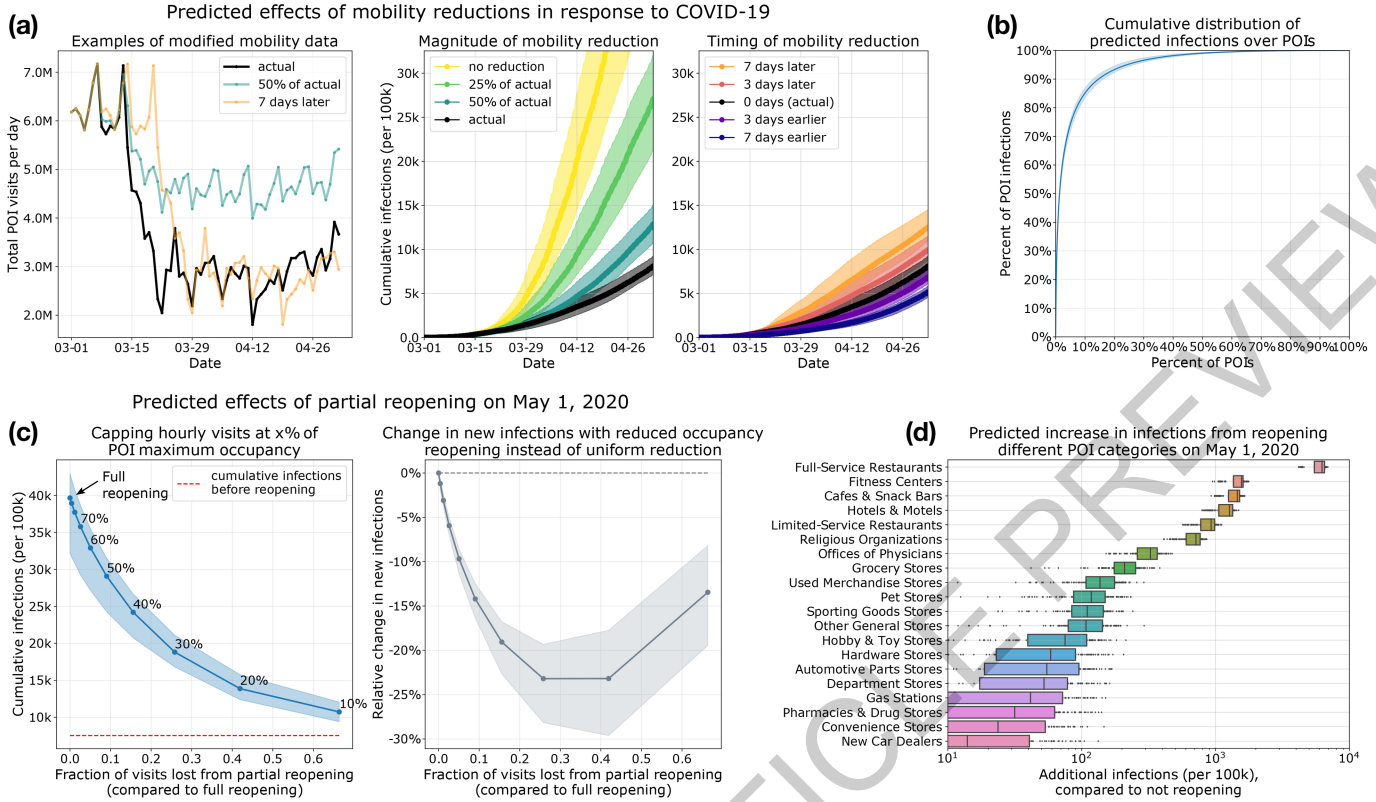

Figure 2 | Assessing mobility reduction and reopening. The Chicago metro area is used as an example, but references to results for all metro areas are provided for each subfigure. **(a)** Counterfactual simulations (left) of past mobility reduction illustrate that the magnitude of reduction (middle) was at least as important as its timing (right) (Tables S4–S5). **(b)** The model predicts that most infections at POIs occur at a small fraction of "super-spreader" POIs (Figure S10). **(c)** Left: We plot cumulative predicted infections after one month of reopening against the fraction of visits lost by partial instead of full reopening (ED Figure 3); the annotations within the plot show the fraction of maximum occupancy used as the cap. Compared to full reopening, capping at 20% maximum occupancy in Chicago cuts down new infections by more than 80%, while only losing 42% of overall visits. Right: Compared to uniformly reducing visits, the reduced maximum occupancy strategy always results in a smaller predicted increase in infections for the same number of visits (ED Figure 4). The y-axis plots the relative difference between the predicted number of new infections under the reduced occupancy strategy compared to uniform reduction. **(d)** Reopening full-service restaurants has the largest predicted impact on infections, due to the large number of restaurants as well as their high visit densities and long dwell times (Figures S15–S24). Colors are used to distinguish the different POI categories, but do not have any additional meaning. All results in this figure are aggregated across 4 parameter sets and 30 stochastic realizations (N = 120). Shaded regions in (a–c) denote the 2.5th–97.5th percentiles; boxes in (d) denote the interquartile range, with data points outside the range individually shown.

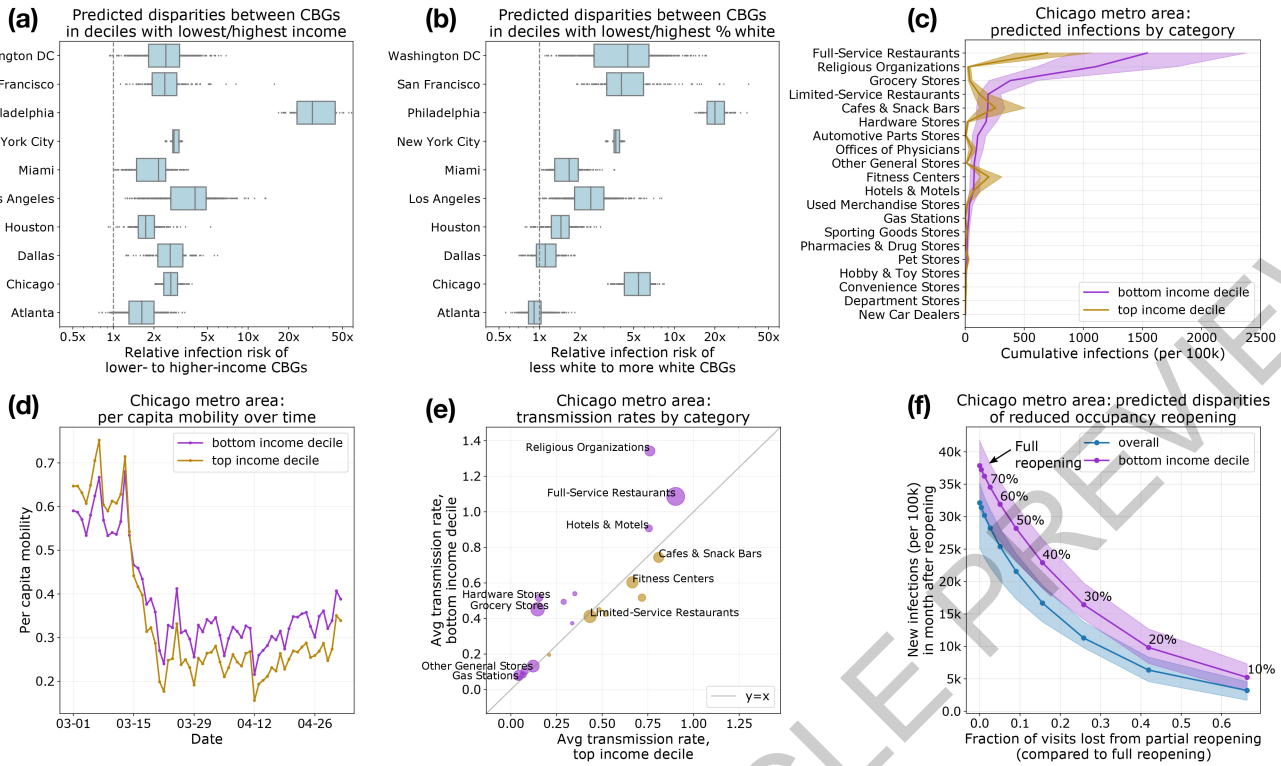

Figure 3 | Mobility patterns give rise to infection disparities. For (c–f), the Chicago metro area is used as an example, but references to results for all metro areas are provided for each subfigure. **(a)** In every metro area, our model predicts that people in lower-income CBGs are likelier to be infected. **(b)** People in non-white CBGs area are also likelier to be infected, although results are more variable across metro areas. **(c)** The overall predicted disparity is driven by a few POI categories like full-service restaurants (Figure S2). **(d)** One reason for the predicted disparities is that higher-income CBGs were able to reduce their mobility levels below those of lower-income CBGs (ED Figure 6). **(e)** Within each POI category, people from lower-income CBGs tend to visit POIs that have higher predicted transmission rates (ED Table 3). The size of each dot represents the average number of visits per capita made to the category. The top 10 out of 20 categories with the most visits are labeled, covering 0.48–2.88 visits per capita (Hardware Stores–Full-Service Restaurants). **(f)** Reopening (at different levels of reduced maximum occupancy) leads to more predicted infections in lower-income CBGs than in the overall population (ED Figure 3). In (c–f), purple denotes lower-income CBGs, yellow denotes higher-income CBGs, and blue represents the overall population. Aside from (d) and (e), which were directly extracted from mobility data, all results in this figure represent predictions aggregated over model realizations. Across metro areas, we sample 97 parameter sets, with 30 stochastic realizations each (N = 2,910); see Table S6 for the number of sets per metro area. Shaded regions in (c) and (f) denote the 2.5th–97.5th percentiles; boxes in (a–b) denote the interquartile range, with data points outside the range individually shown.

Methods

The Methods section is structured as follows. We describe the datasets we use in Methods M1 and the mobility network that we derive from these datasets in Methods M2. In Methods M3, we discuss the SEIR model we overlay on the mobility network; in Methods M4, we describe how we calibrate this model and quantify uncertainty in its predictions. Finally, in Methods M5, we provide details on the experimental procedures used for our analyses of mobility reduction, reopening plans, and demographic disparities.

M1 Datasets

SafeGraph. We use data provided by SafeGraph, a company that aggregates anonymized location data from numerous mobile applications. SafeGraph data captures the movement of people between census block groups (CBGs), which are geographical units that typically contain a population of between 600 and 3,000 people, and points of interest (POIs) like restaurants, grocery stores, or religious establishments. Specifically, we use the following SafeGraph datasets:

1. Places Patterns[39] and Weekly Patterns (v1)[40]. These datasets contain, for each POI, hourly counts of the number of visitors, estimates of median visit duration in minutes (the "dwell time"), and aggregated weekly and monthly estimates of visitors' home CBGs. We use visitor home CBG data from the Places Patterns dataset, as described below: for privacy reasons, SafeGraph excludes a home CBG from this dataset if fewer than 5 devices were recorded at the POI from that CBG over the course of the month. For each POI, SafeGraph also provides their North American Industry Classification System (NAICS) category, as well as estimates of its median visit duration in minutes and physical area in square feet. (Area is computed using the footprint polygon SafeGraph assigns to the POI[41,42].) We analyze Places Patterns data from January 1, 2019 to February 29, 2020 and Weekly Patterns data from March 1, 2020 to May 2, 2020.

2. Social Distancing Metrics[43], which contains daily estimates of the proportion of people staying home in each CBG. We analyze Social Distancing Metrics data from March 1, 2020 to May 2, 2020.

We focus on 10 of the largest metropolitan statistical areas in the US (Extended Data Table 1). We chose these metro area s by taking a random subset of the SafeGraph Patterns data and picking the 10 metro area s with the most POIs in the data. Our methods in this paper can be straightforwardly applied, in principle, to the other metro area s in the original SafeGraph data. For each metro area, we include all POIs that meet all of the following requirements: (1) the POI is located in the metro area ; (2) SafeGraph has visit data for this POI for every hour that we model, from 12 am on March 1, 2020 to 11 pm on May 2, 2020; (3) SafeGraph has recorded the home CBGs of this POI's visitors for at least one month from January 2019 to February 2020; (4) the POI is not a "parent" POI. "Parent" POIs comprise a small fraction of POIs in the dataset which overlap and include the visits from their "child" POIs: for example, many malls in the dataset are parent POIs which include the visits from stores which are their child POIs. To avoid double-counting visits, we remove all parent POIs from the dataset. After applying these POI filters, we include all CBGs that have at least 1 recorded visit to at least 10 of the remaining POIs; this means that CBGs from outside the metro area may be included if they visit this metro area frequently enough. Summary statistics of the post-processed data are in Extended Data Table 1. Overall, we analyze 57k CBGs from the 10 metro area s, and over 310 M visits from these CBGs to nearly 553k POIs.

SafeGraph data has been used to study consumer preferences[44] and political polarization[45]. More recently, it has been used as one of the primary sources of mobility data in the US for tracking the effects of the SARS-CoV-2 pandemic[26,28,46–48]. In SI Methods Section 1, we show that aggregate trends in SafeGraph mobility data match up to aggregate trends in Google mobility data in the US[49], before and after the imposition of stay-at-home measures. Previous analyses of SafeGraph data have shown that it is geographically representative: for example, it does not systematically over-represent individuals from CBGs in different counties or with different racial compositions, income levels, or educational levels[50,51].

US Census. Our data on the demographics of census block groups (CBGs) comes from the US Census Bureau's American Community Survey (ACS)[52]. We use the 5-year ACS (2013–2017) to extract the median household income, proportion of white residents, and proportion of black residents of each CBG. For the total population of each CBG, we use the most recent one-year estimates (2018); one-year estimates are noisier but we wish to minimize systematic downward bias in our total population counts (due to population growth) by making them as recent as possible.

New York Times. We calibrate our models using the COVID-19 dataset published by the *The New York Times*[32]. Their dataset consists of cumulative counts of cases and deaths in the United States over time, at the state and county level. For each metro area that we model, we sum over the county-level counts to produce overall counts for the entire metro area. We convert the cumulative case and death counts to daily counts for the purposes of model calibration, as described in Methods M4.

Data ethics. The dataset from *The New York Times* consists of aggregated COVID-19 confirmed case and death counts collected by journalists from public news conferences and public data releases. For the mobility data, consent was obtained by the third-party sources collecting the data. SafeGraph aggregates data from mobile applications that obtain opt-in consent from their users to collect anonymous location data. Google's mobility data consists of aggregated, anonymized sets of data from users who have chosen to turn on the Location History setting. Additionally, we obtained IRB exemption for SafeGraph data from the Northwestern University IRB office.

M2 Mobility network

Definition. We consider a complete undirected bipartite graph $\mathcal{G} = (\mathcal{V}, \mathcal{E})$ with time-varying edges. The vertices $\mathcal{V}$ are partitioned into two disjoint sets $\mathcal{C} = \{c_1, \ldots, c_m\}$, representing m census block groups (CBGs), and $\mathcal{P} = \{p_1, \ldots, p_n\}$, representing n points of interest (POIs). From US Census data, each CBG c_i is labeled with its population N_{c_i}, income distribution, and racial and age demographics. From SafeGraph data, each POI p_j is similarly labeled with its category (e.g., restaurant, grocery store, or religious organization), its physical size in square feet a_{p_j}, and the median dwell time d_{p_j} of visitors to p_j. The weight $w_{ij}^{(t)}$ on an edge (c_i, p_j) at time t represents our estimate of the number of individuals from CBG c_i visiting POI p_j at the t-th hour of simulation. We record the number of edges (with non-zero weights) in each metro area and over all hours from March 1, 2020 to May 2, 2020 in Extended Data Table 1. Across all 10 metro area s, we study 5.4 billion edges between 56,945 CBGs and 552,758 POIs.

Network estimation (overview). The central technical challenge in constructing this network is estimating the network weights $W^{(t)} = \{w_{ij}^{(t)}\}$ from SafeGraph data, since this visit matrix is not directly available from the data. Our general methodology for network estimation is as follows:

1. From SafeGraph data, we can derive a time-independent estimate $\overline{W}$ of the visit matrix that captures the aggregate distribution of visits from CBGs to POIs from January 2019 to February 2020.

2. However, visit patterns differ substantially from hour to hour (e.g., day versus night) and day to day (e.g., pre- versus post-lockdown). To capture these variations, we use current SafeGraph data to estimate the CBG marginals $U^{(t)}$, i.e., the number of people in each CBG who are out visiting POIs at hour t, as well as the POI marginals $V^{(t)}$, i.e., the total number of visitors present at each POI p_j at hour t.

3. We then apply the iterative proportional fitting procedure (IPFP) to estimate an hourly visit matrix $W^{(t)}$ that is consistent with the hourly marginals $U^{(t)}$ and $V^{(t)}$ but otherwise "as similar as possible" to the distribution of visits in the aggregate visit matrix $\overline{W}$, in terms of Kullback-Leibler divergence.

IPFP is a classic statistical method[31] for adjusting joint distributions to match pre-specified marginal distributions, and it is also known in the literature as biproportional fitting, the RAS algorithm, or raking[53]. In the social sciences, it has been widely used to infer the characteristics of local subpopulations (e.g., within each CBG) from aggregate data[54–56]. IPFP estimates the joint distribution of visits from CBGs to POIs by alternating between scaling each row to match the hourly row (CBG) marginals $U^{(t)}$ and scaling each column to match the hourly column (POI) marginals $V^{(t)}$. For further details about the estimation procedure, we refer the reader to SI Methods Section 3.

M3 Model dynamics

To model the spread of SARS-CoV-2, we overlay a metapopulation disease transmission model on the mobility network defined in Methods M2. The transmission model structure follows prior work on epidemiological models of SARS-CoV-2[15,20] but incorporates a fine-grained mobility network into the calculations of the transmission rate. We construct separate mobility networks and models for each metropolitan statistical area.

We use a SEIR model with susceptible (S), exposed (E), infectious (I), and removed (R) compartments. Susceptible individuals have never been infected, but can acquire the virus through contact with infectious individuals, which may happen at POIs or in their home CBG. They then enter the exposed state, during which they have been infected but are not infectious yet. Individuals transition from exposed to infectious at a rate inversely proportional to the mean latency period. Finally, they transition into the removed state at a rate inversely proportional to the mean infectious period. The removed state represents individuals who can no longer be infected or infect others, e.g., because they have recovered, self-isolated, or died.

Each CBG c_i maintains its own SEIR instantiation, with $S_{c_i}^{(t)}$, $E_{c_i}^{(t)}$, $I_{c_i}^{(t)}$, and $R_{c_i}^{(t)}$ representing how many individuals in CBG c_i are in each disease state at hour t, and $N_{c_i} = S_{c_i}^{(t)} + E_{c_i}^{(t)} + I_{c_i}^{(t)} + R_{c_i}^{(t)}$. At each hour t, we sample the transitions between states as follows:

$$N_{S_{c_i}\to E_{c_i}}^{(t)} \sim \text{Pois}\left(\frac{S_{c_i}^{(t)}}{N_{c_i}} \sum_{j=1}^{n} \lambda_{p_j}^{(t)} w_{ij}^{(t)}\right) + \text{Binom}\left(S_{c_i}^{(t)}, \lambda_{c_i}^{(t)}\right) \quad (1)$$

$$N_{E_{c_i}\to I_{c_i}}^{(t)} \sim \text{Binom}\left(E_{c_i}^{(t)}, 1/\delta_E\right) \quad (2)$$

$$N_{I_{c_i}\to R_{c_i}}^{(t)} \sim \text{Binom}\left(I_{c_i}^{(t)}, 1/\delta_I\right), \quad (3)$$

where $\lambda_{p_j}^{(t)}$ is the rate of infection at POI p_j at time t; $w_{ij}^{(t)}$, the ij-th entry of the visit matrix from the mobility network (Methods M2), is the number of visitors from CBG c_i to POI p_j at time t; $\lambda_{c_i}^{(t)}$ is the base rate of infection that is independent of visiting POIs; δ_E is the mean latency period; and δ_I is the mean infectious period.

We then update each state to reflect these transitions. Let $\Delta S_{c_i}^{(t)} := S_{c_i}^{(t+1)} - S_{c_i}^{(t)}$, and likewise for $\Delta E_{c_i}^{(t)}$, $\Delta I_{c_i}^{(t)}$, and $\Delta R_{c_i}^{(t)}$. Then,

$$\Delta S_{c_i}^{(t)} := -N_{S_{c_i}\to E_{c_i}}^{(t)} \quad (4)$$

$$\Delta E_{c_i}^{(t)} := N_{S_{c_i}\to E_{c_i}}^{(t)} - N_{E_{c_i}\to I_{c_i}}^{(t)} \quad (5)$$

$$\Delta I_{c_i}^{(t)} := N_{E_{c_i}\to I_{c_i}}^{(t)} - N_{I_{c_i}\to R_{c_i}}^{(t)} \quad (6)$$

$$\Delta R_{c_i}^{(t)} := N_{I_{c_i}\to R_{c_i}}^{(t)}. \quad (7)$$

M3.1 The number of new exposures $N_{S_{c_i}\to E_{c_i}}^{(t)}$. We separate the number of new exposures $N_{S_{c_i}\to E_{c_i}}^{(t)}$ in CBG c_i at time t into two parts: cases from visiting POIs, which are sampled from $\text{Pois}((S_{c_i}^{(t)}/N_{c_i})\sum_{j=1}^{n}\lambda_{p_j}^{(t)}w_{ij}^{(t)})$, and other cases not captured by visiting POIs, which are sampled from $\text{Binom}(S_{c_i}^{(t)}, \lambda_{c_i}^{(t)})$.

New exposures from visiting POIs. We assume that any susceptible visitor to POI p_j at time t has the same independent probability $\lambda_{p_j}^{(t)}$ of being infected and transitioning from the susceptible (S) to the exposed (E) state. Since there are $w_{ij}^{(t)}$ visitors from CBG c_i to POI p_j at time t, and we assume that a $S_{c_i}^{(t)}/N_{c_i}$ fraction of them are susceptible, the number of new exposures among these visitors is distributed as $\text{Binom}(w_{ij}^{(t)}S_{c_i}^{(t)}/N_{c_i}, \lambda_{p_j}^{(t)}) \approx \text{Pois}(\lambda_{p_j}^{(t)}w_{ij}^{(t)}S_{c_i}^{(t)}/N_{c_i})$. The number of new exposures among all outgoing visitors from CBG c_i is therefore distributed as the sum of the above expression over all POIs, $\text{Pois}((S_{c_i}^{(t)}/N_{c_i})\sum_{j=1}^{n}\lambda_{p_j}^{(t)}w_{ij}^{(t)})$.

We model the infection rate at POI p_j at time t, $\lambda_{p_j}^{(t)} := \beta_{p_j}^{(t)} \cdot I_{p_j}^{(t)}/V_{p_j}^{(t)}$, as the product of its transmission rate $\beta_{p_j}^{(t)}$ and proportion of infectious individuals $I_{p_j}^{(t)}/V_{p_j}^{(t)}$, where $V_{p_j}^{(t)} := \sum_{i=1}^{m} w_{ij}^{(t)}$ is the total number of visitors to p_j at time t. We model the transmission rate at POI p_j at time t as

$$\beta_{p_j}^{(t)} := \psi \cdot d_{p_j}^2 \cdot \frac{V_{p_j}^{(t)}}{a_{p_j}}, \quad (8)$$

where a_{p_j} is the physical area of p_j, and ψ is a transmission constant (shared across all POIs) that we fit to data. The inverse scaling of transmission rate with area a_{p_j} is a standard simplifying assumption[57]. The dwell time fraction $d_{p_j} \in [0, 1]$ is what fraction of an hour an average visitor to p_j at any hour will spend there (SI Methods Section 3); it has a quadratic effect on the POI transmission rate $\beta_{p_j}^{(t)}$ because it reduces both (1) the time that a susceptible visitor spends at p_j and (2) the density of visitors at p_j. With this expression for the transmission rate $\beta_{p_j}^{(t)}$, we can calculate the infection rate at POI p_j at time t as

$$\lambda_{p_j}^{(t)} = \beta_{p_j}^{(t)} \cdot \frac{I_{p_j}^{(t)}}{V_{p_j}^{(t)}} = \psi \cdot d_{p_j}^2 \cdot \frac{I_{p_j}^{(t)}}{a_{p_j}}. \quad (9)$$

For sufficiently large values of ψ and a sufficiently large proportion of infected individuals, the expression above can sometimes exceed 1. To address this, we simply clip the infection rate to 1. However, this occurs very rarely for the parameter settings and simulation duration that we use.

Finally, to compute the number of infectious individuals at p_j at time t, $I_{p_j}^{(t)}$, we assume that the proportion of infectious individuals among the $w_{kj}^{(t)}$ visitors to p_j from a CBG c_k mirrors the overall density of infections $I_{c_k}^{(t)}/N_{c_k}$ in that CBG, although we note that the scaling factor ψ can account for differences in the ratio of infectious individuals who visit POIs. This gives

$$I_{p_j}^{(t)} := \sum_{k=1}^{m} \frac{I_{c_k}^{(t)}}{N_{c_k}} w_{kj}^{(t)}. \quad (10)$$

Base rate of new exposures not captured by visiting POIs. In addition to the new exposures from infections at POIs, we model a CBG-specific base rate of new exposures that is independent of POI visit activity. This captures other sources of infections, e.g., household infections or infections at POIs that are absent from the SafeGraph data. We assume that at each hour, every susceptible individual in CBG c_i has a base probability $\lambda_{c_i}^{(t)}$ of becoming infected and transitioning to the exposed state, where

$$\lambda_{c_i}^{(t)} := \beta_{\text{base}} \cdot \frac{I_{c_i}^{(t)}}{N_{c_i}} \quad (11)$$

is the product of the base transmission rate β_{base} and the proportion of infectious individuals in CBG c_i. β_{base} is a constant (shared across all CBGs) that we fit to data.

Overall number of new exposures. Putting all of the above together yields the expression for the distribution of new exposures in CBG c_i at time t,

$$\begin{aligned} N^{(t)}_{S_{c_i}\to E_{c_i}} &\sim \text{Pois}\left(\frac{S^{(t)}_{c_i}}{N_{c_i}}\sum_{j=1}^{n}\lambda^{(t)}_{p_j}w^{(t)}_{ij}\right) + \text{Binom}(S^{(t)}_{c_i}, \lambda^{(t)}_{c_i}) \\ &= \underbrace{\text{Pois}\left(\psi\cdot\frac{S^{(t)}_{c_i}}{N_{c_i}}\cdot\sum_{j=1}^{n}\frac{d^2_{p_j}}{a_{p_j}}\left(\sum_{k=1}^{m}\frac{I^{(t)}_{c_k}}{N_{c_k}}w^{(t)}_{kj}\right)w^{(t)}_{ij}\right)}_{\text{new infections from visiting POIs}} \\ &\quad + \underbrace{\text{Binom}\left(S^{(t)}_{c_i}, \beta_{\text{base}}\cdot\frac{I^{(t)}_{c_i}}{N_{c_i}}\right)}_{\text{base rate of new CBG infections}}. \end{aligned} \tag{12}$$

M3.2 The number of new infectious and removed cases. We model exposed individuals as becoming infectious at a rate inversely proportional to the mean latency period δ_E. At each time step t, we assume that each exposed individual has a constant, time-independent probability of becoming infectious, with

$$N^{(t)}_{E_{c_i}\to I_{c_i}} \sim \text{Binom}(E^{(t)}_{c_i}, 1/\delta_E). \tag{13}$$

Similarly, we model infectious individuals as transitioning to the removed state at a rate inversely proportional to the mean infectious period δ_I, with

$$N^{(t)}_{I_{c_i}\to R_{c_i}} \sim \text{Binom}(I^{(t)}_{c_i}, 1/\delta_I), \tag{14}$$

We estimate $\delta_E = 96$ hours[20,58] and $\delta_I = 84$ hours[20] from prior literature.

M3.3 Model initialization. In our experiments, $t = 0$ is the first hour of March 1, 2020. We approximate the infectious I and removed R compartments at $t = 0$ as initially empty, with all infected individuals in the exposed E compartment. We further assume the same expected initial prevalence p_0 in every CBG c_i. At $t = 0$, every individual in the metro area has the same independent probability p_0 of being exposed E instead of susceptible S. We thus initialize the model state by setting

$$S^{(0)}_{c_i} = N_{c_i} - E^{(0)}_{c_i} \tag{15}$$

$$E^{(0)}_{c_i} \sim \text{Binom}(N_{c_i}, p_0) \tag{16}$$

$$I^{(0)}_{c_i} = 0 \tag{17}$$

$$R^{(0)}_{c_i} = 0. \tag{18}$$

M3.4 Aggregate mobility and no-mobility baseline models

Comparison to aggregate mobility model. Our model uses a detailed mobility network to simulate disease spread. To test if this detailed model is necessary, or if our model is simply making use of aggregate mobility patterns, we tested an alternate SEIR model that uses the aggregate number of visits made to any POI in the metro area in each hour, but not the breakdown of visits between specific CBGs to specific POIs. Like our model, the aggregate mobility model also captures new cases from visiting POIs and a base rate of infection that is independent of POI visit activity; thus, the two models have the same three free parameters (ψ, scaling transmission rates at POIs; β_{base}, the base transmission rate; and p_0, the initial fraction of infected individuals). However, instead of having POI-specific rates of infection, the aggregate mobility model only captures a single probability that a susceptible person from any CBG will become infected due to a visit to any POI at time t; we make this simplification because the aggregate mobility model no longer has access to the breakdown of visits between CBGs and POIs. This probability $\lambda^{(t)}_{POI}$ is defined as

$$\lambda^{(t)}_{POI} = \psi\cdot\underbrace{\frac{\sum_{i=1}^{m}\sum_{j=1}^{n}w^{(t)}_{ij}}{nm}}_{\text{average mobility at time } t}\cdot\frac{I^{(t)}}{N}, \tag{19}$$

where m is the number of CBGs, n is the number of POIs, $I^{(t)}$ is the total number of infectious individuals at time t, and N is the total population size of the metro area. For the base rate of infections in CBGs, we assume the same process as in our network model: the probability $\lambda^{(t)}_{c_i}$ that a susceptible person in CBG c_i will become infected in their CBG at time t is equal to β_{base} times the current infectious fraction of c_i (Equation 11). Putting it together, the aggregate mobility model defines the number of new exposures in CBG c_i at time t as

$$N^{(t)}_{S_{c_i}\to E_{c_i}} \sim \underbrace{\text{Binom}(S^{(t)}_{c_i}, \lambda^{(t)}_{POI})}_{\text{new infections from visiting POIs}} + \underbrace{\text{Binom}(S^{(t)}_{c_i}, \lambda^{(t)}_{c_i})}_{\text{base rate of new CBG infections}}. \tag{20}$$

All other dynamics remain the same between the aggregate mobility model and our network model, and we calibrated the models in the same way, which we will describe in Methods M4. We found that our network model substantially outperformed the aggregate mobility model in out-of-sample cases prediction: on average across metro areas, our best-fit network model's out-of-sample RMSE was only 58% that of the best-fit aggregate mobility model (Extended Data Figure 1). This demonstrates that it is not only general mobility patterns, but specifically the mobility *network* that allows our model to accurately fit observed cases.

Comparison to baseline that does not use mobility data. To determine the extent to which mobility data might aid in modeling the case trajectory, we also compared our model to a baseline SEIR model that does not use mobility data and simply assumes that all individuals within an metro area mix uniformly. In this no-mobility baseline, an individual's risk of being infected and transitioning to the exposed state at time t is

$$\lambda^{(t)} := \beta_{\text{base}}\cdot\frac{I^{(t)}}{N}, \tag{21}$$

where $I^{(t)}$ is the total number of infectious individuals at time t, and N is the total population size of the metro area. As above, the other model dynamics are identical, and for model calibration we performed a similar grid search over β_{base} and p_0. As expected, we found both the network and aggregate mobility models outperformed the no-mobility model on out-of-sample case predictions (Extended Data Figure 1).

M4 Model calibration and validation

Most of our model parameters can either be estimated from SafeGraph and US Census data, or taken from prior work (see Extended Data Table 2 for a summary). This leaves 3 model parameters that do not have direct analogues in the literature, and that we therefore need to calibrate with data:

1. The transmission constant in POIs, ψ (Equation (9))
2. The base transmission rate, β_{base} (Equation (11))
3. The initial proportion of exposed individuals at time $t = 0$, p_0 (Equation (16)).

In this section, we describe how we fit these parameters to published numbers of confirmed cases, as reported by *The New York Times*. We fit models for each metro area separately.

M4.1 Selecting parameter ranges

Transmission rate factors ψ and β_{base}. We select parameter ranges for the transmission rate factors ψ and β_{base} by checking if the model

outputs match plausible ranges of the basic reproduction number R_0 pre-lockdown, since R_0 has been the study of substantial prior work on SARS-CoV-2[59]. Under our model, we can decompose $R_0 = R_{base} + R_{POI}$, where R_{POI} describes transmission due to POIs and R_{base} describes the remaining transmission (as in Equation (12)). We first establish plausible ranges for R_{base} and R_{POI} before translating these into plausible ranges for β_{base} and ψ.

We assume that R_{base} ranges from 0.1–2. R_{base} models transmission that is not correlated with activity at POIs in the SafeGraph dataset, including within-household transmission and transmission at POI categories which are not well-captured in the SafeGraph dataset. We chose the lower limit of 0.1 because beyond that point, base transmission would only contribute minimally to overall R, whereas previous work suggests that within-household transmission is a substantial contributor to overall transmission[60–62]. Household transmission alone is not estimated to be sufficient to tip overall R_0 above 1; for example, a single infected individual has been estimated to cause an average of 0.32 (0.22, 0.42) secondary within-household infections[60]. However, because R_{base} may also capture transmission at POIs not captured in the SafeGraph dataset, to be conservative, we chose an upper limit of $R_{base} = 2$; as we describe below, the best-fit models for all 10 metro area s have $R_{base} < 2$, and 9 out of 10 have $R_{base} < 1$. We allow R_{POI} to range from 1–3, which corresponds to allowing $R_0 = R_{POI} + R_{base}$ to range from 1.1–5. This is a conservatively wide range, since prior work estimates a pre-lockdown R_0 of 2–3[59].

To determine the values of R_{base} and R_{POI} that a given pair of β_{base} and ψ imply, we seeded a fraction of index cases and then ran the model on looped mobility data from the first week of March to capture pre-lockdown conditions. We initialized the model by setting p_0, the initial proportion of exposed individuals at time $t = 0$, to $p_0 = 10^{-4}$, and then sampling in accordance with Equation (16). Let N_0 be the number of initial exposed individuals sampled. We computed the number of individuals that these N_0 index cases went on to infect through base transmission, N_{base}, and POI transmission, N_{POI}, which gives

$$R_{POI} = \frac{N_{POI}}{N_0} \tag{22}$$

$$R_{base} = \frac{N_{base}}{N_0}. \tag{23}$$

We averaged these quantities over stochastic realizations for each metro area. Figure S6 shows that, as expected, R_{base} is linear in β_{base} and R_{POI} is linear in ψ. R_{base} lies in the plausible range when β_{base} ranges from 0.0012–0.024, and R_{POI} lies in the plausible range (for at least one metro area) when ψ ranges from 515–4,886, so these are the parameter ranges we consider when fitting the model. As described in Methods M4.2, we verified that case count data for all metro area s can be fit using parameter settings for β_{base} and ψ within these ranges.

Initial prevalence of exposures, p_0. The extent to which SARS-CoV-2 infections had spread in the US by the start of our simulation (March 1, 2020) is currently unclear[63]. To account for this uncertainty, we allow p_0 to vary across a large range between 10^{-5} and 10^{-2}. As described in Methods M4.2, we verified that case count data for all metro area s can be fit using parameter settings for p_0 within this range.

M4.2 Fitting to the number of confirmed cases. Using the parameter ranges above, we grid searched over ψ, β_{base}, and p_0 to find the models that best fit the number of confirmed cases reported by *The New York Times* (NYT)[32]. For each metro area, we tested 1,500 different combinations of ψ, β_{base}, and p_0 in the parameter ranges specified above, with parameters linearly spaced for ψ and β_{base} and logarithmically spread for p_0.

In Methods M3, we directly model the number of infections but not the number of confirmed cases. To estimate the number of confirmed cases, we assume that an $r_c = 0.1$[20,58,64–66] proportion of infections will be confirmed, and moreover that they will confirmed exactly $\delta_c = 168$ hours (7 days)[20,66] after becoming infectious. From these assumptions, we can calculate the predicted number of newly confirmed cases across all CBGs in the metro area on day d,

$$N_{cases}^{(\text{day } d)} = r_c \cdot \sum_{i=1}^{m} \sum_{\tau=24(d-1)+1-\delta_c}^{24d-\delta_c} N_{E_{c_i} \to I_{c_i}}^{(\tau)}, \tag{24}$$

where m indicates the total number of CBGs in the metro area and for convenience we define $N_{E_{c_i} \to I_{c_i}}^{(\tau)}$, the number of newly infectious people at hour τ, to be 0 when $\tau < 1$.

From NYT data, we have the reported number of new cases $\hat{N}_{cases}^{(\text{day } d)}$ for each day d, summed over each county in the metro area. We compare the reported number of cases and the number of cases that our model predicts by computing the root-mean-squared-error (RMSE) between each of the $D = \square T/24 \square$ days of our simulations,

$$\text{RMSE} = \sqrt{\frac{1}{D} \sum_{d=1}^{D} (N_{cases}^{(\text{day } d)} - \hat{N}_{cases}^{(\text{day } d)})^2}. \tag{25}$$

For each combination of model parameters and for each metro area, we quantify model fit with the NYT data by running 30 stochastic realizations and averaging their RMSE. Note that we measure model fit based on the daily number of new reported cases (as opposed to the cumulative number of reported cases)[67].

Our simulation spans March 1 to May 2, 2020, and we use mobility data from that period. However, because we assume that cases will be confirmed $\delta_c = 7$ days after individuals become infectious, we predict the number of cases with a 7 day offset, from March 8 to May 9, 2020.

M4.3 Parameter selection and uncertainty quantification. Throughout this paper, we report aggregate predictions from different parameter sets of ψ,β_{base}, and p_0 and multiple stochastic realizations. For each metro area, we:

1. Find the best-fit parameter set, i.e., with the lowest average RMSE on daily incident cases over stochastic realizations.
2. Select all parameter sets that achieve an RMSE (averaged over stochastic realizations) within 20% of the RMSE of the best-fit parameter set.
3. Pool together all predictions across those parameter sets and all of their stochastic realizations, and report their mean and 2.5th/97.5th percentiles.

On average, each metro area has 9.7 parameter sets that achieve an RMSE within 20% of the best-fitting parameter set (Table S6). For each parameter set, we have results for 30 stochastic realizations.

This procedure corresponds to rejection sampling in an Approximate Bayesian Computation framework[15], where we assume an error model that is Gaussian with constant variance; we pick an acceptance threshold based on what the best-fit model achieves; and we use a uniform parameter grid instead of sampling from a uniform prior. It quantifies uncertainty from two sources. First, the multiple realizations capture stochastic variability between model runs with the same parameters. Second, simulating with all parameter sets that are within 20% of the RMSE of the best fit captures uncertainty in the model parameters ψ, β_{base}, and p_0. The latter is equivalent to assuming that the posterior probability over the true parameters is uniformly spread among all parameter sets within the 20% threshold.

M4.4 Model validation on out-of-sample cases. We validate our models by showing that they predict the number of confirmed cases on out-of-sample data when we have access to corresponding mobility data. For each metro area, we split the available NYT dataset into a training set (spanning March 8, 2020 to April 14, 2020) and a test set (spanning April 15, 2020 to May 9, 2020). We fit the model parameters

ψ, β_{base}, and p_0, as described in Methods M4.2, but only using the training set. We then evaluate the predictive accuracy of the resulting model on the test set. When running our models on the test set, we still use mobility data from the test period. Thus, this is an evaluation of whether the models can accurately predict the number of cases, given mobility data, in a time period that was not used for model calibration. Extended Data Figure 1 shows that our network model fits the out-of-sample case data fairly well, and that our model substantially outperforms alternate models that use aggregated mobility data (without a network) or do not use mobility data at all (Methods M3.4). Note that we only use this train/test split to evaluate out-of-sample model accuracy. All other results are generated using parameter sets that best fit the *entire* dataset, as described above.

M5 analysis details

In this section, we include additional details about the experiments underlying the figures in the paper. We omit explanations for figures that are completely described in the main text.

Counterfactuals of mobility reduction (Figure 2a, Tables S4–S5). To simulate what would have happened if we changed the magnitude or timing of mobility reduction, we modify the real mobility networks from March 1–May 2, 2020, and then run our models on the hypothetical data. In Figure 2a, we report the total number of people per 100k population ever infected (i.e., in the exposed, infectious, and removed states) by the end of the simulation.

To simulate a smaller magnitude of mobility reduction, we interpolate between the mobility network from the first week of simulation (March 1–7, 2020), which we use to represent typical mobility levels, and the actual observed mobility network for each week. Let $W^{(t)}$ represent the observed visit matrix at the t-th hour of simulation, and let $f(t) = t \bmod 168$ map t to its corresponding hour in the first week of simulation, since there are 168 hours in a week. To represent the scenario where people had committed to $\alpha \in [0, 1]$ times the actual observed reduction in mobility, we construct a visit matrix $\tilde{W}_{\alpha}^{(t)}$ that is an α-convex combination of $W^{(t)}$ and $W^{f(t)}$,

$$\tilde{W}_{\alpha}^{(t)} := \alpha W^{(t)} + (1-\alpha) W^{f(t)}. \tag{26}$$

If α is 1, then $\tilde{W}_{\alpha}^{(t)} = W^{(t)}$, and we use the actual observed mobility network for the simulation. On the other hand, if $\alpha = 0$, then $\tilde{W}_{\alpha}^{(t)} = W^{f(t)}$, and we assume that people did not reduce their mobility levels at all by looping the visit matrix for the first week of March throughout the simulation. Any other $\alpha \in [0, 1]$ interpolates between these two extremes.

To simulate changing the timing of mobility reduction, we shift the mobility network by $d \in [-7, 7]$ days. Let T represent the last hour in our simulation (May 2, 2020, 11 PM), let $f(t) = t \bmod 168$ map t to its corresponding hour in the first week of simulation as above, and similarly let $g(t)$ map t to its corresponding hour in the last week of simulation (April 27–May 2, 2020). We construct the time-shifted visit matrix $\widetilde{W}_{d}^{(t)}$

$$\widetilde{W}_{d}^{(t)} := \begin{cases} W^{(t-24d)} & \text{if } 0 \le t - 24d \le T, \\ W^{f(t-24d)} & \text{if } t - 24d < 0, \\ W^{g(t-24d)} & \text{otherwise.} \end{cases} \tag{27}$$

If d is positive, this corresponds to starting mobility reduction d days later; if we imagine time on a horizontal line, this shifts the time series to the right by $24d$ hours. However, doing so leaves the first $24d$ hours without visit data, so we fill it in by reusing visit data from the first week of simulation. Likewise, if d is negative, this corresponds to starting mobility reduction d days earlier, and we fill in the last $24d$ hours with visit data from the last week of simulation.

Distribution of predicted infections over POIs (Figures 2b, Extended Data 2, S10). We run our models on the observed mobility data from March 1–May 2, 2020 and record the number of predicted infections that occur at each POI. Specifically, for each hour t, we compute the number of expected infections that occur at each POI p_j by taking the number of susceptible people who visit p_j in that hour multiplied by the POI infection rate $\lambda_{p_j}^{(t)}$ (Equation (9)). In Figures 2b and S10, we sort the POIs by their total predicted number of infections (summed over hours) and plot the cumulative distribution of infections over this ordering of POIs. In Extended Data Figure 2, we select the POI categories that contribute the most to predicted infections and plot the daily proportion of POI infections each category accounted for (summed over POIs within the category) over time.

Reducing mobility by capping maximum occupancy (Figures 2c, Extended Data 3). We implemented two partial reopening strategies: one that uniformly reduced visits at POIs to a fraction of full activity, and the other that "capped" each POI's hourly visits to a fraction of the POI's maximum occupancy. For each reopening strategy, we started the simulation at March 1, 2020 and ran it until May 31, 2020, using the observed mobility network from March 1–April 30, 2020, and then using a hypothetical post-reopening mobility network from May 1–31, 2020, corresponding to the projected impact of that reopening strategy. Because we only have observed mobility data from March 1–May 2, 2020, we impute the missing mobility data up to May 31, 2020 by looping mobility data from the first week of March, as in the above analysis on the effect of past reductions in mobility. Let T represent the last hour for which we have observed mobility data (May 2, 2020, 11 PM). To simplify notation, we define

$$h(t) := \begin{cases} t & \text{if } t < T, \\ f(t) & \text{otherwise,} \end{cases} \tag{28}$$

where, as above, $f(t) = t \bmod 168$. This function leaves t unchanged if there is observed mobility data at time t, and otherwise maps t to the corresponding hour in the first week of our simulation.

To simulate a reopening strategy that uniformly reduced visits to an γ-fraction of their original level, where $\gamma \in [0, 1]$, we constructed the visit matrix

$$\tilde{W}_{\gamma}^{(t)} := \begin{cases} W^{h(t)} & \text{if } t < \tau, \\ \gamma W^{h(t)} & \text{otherwise,} \end{cases} \tag{29}$$

where τ represents the first hour of reopening (May 1, 2020, 12 AM). In other words, we use the actual observed mobility network up until hour τ, and then subsequently simulate an γ-fraction of full mobility levels.

To simulate the reduced occupancy strategy, we first estimated the maximum occupancy M_{pj} of each POI p_j as the maximum number of visits that it ever had in one hour, across all of March 1 to May 2, 2020. As in previous sections, let $w_{ij}^{(t)}$ represent the i,j-th entry in the observed visit matrix $W^{(t)}$, i.e., the number of people from CBG c_i who visited p_j in hour t, and let $V_{pj}^{(t)}$ represent the total number of visitors to p_j in that hour, i.e., $\sum_i w_{ij}^{(t)}$. We simulated capping at a β-fraction of maximum occupancy, where $\beta \in [0, 1]$, by constructing the visit matrix $\widetilde{W}_{\beta}^{(t)}$ whose i,j-th entry is

$$\tilde{w}_{ij\beta}^{(t)} := \begin{cases} w_{ij}^{h(t)} & \text{if } t < \tau \text{ or } V_{p_j}^{(t)} \le \beta M_{p_j}, \\ \dfrac{\beta M_{p_j}}{V_{p_j}^{(t)}} w_{ij}^{h(t)} & \text{otherwise.} \end{cases} \tag{30}$$

This corresponds to the following procedure: for each POI p_j and time t, we first check if $t < \tau$ (reopening has not started) or if $V_{p_j}^{(t)} \le \beta M_{p_j}$ (the total number of visits to p_j at time t is below the allowed maximum

βM_{p_j}). If so, we leave $w_{ij}^{h(t)}$ unchanged. Otherwise, we compute the scaling factor $\frac{\beta M_{p_j}}{V_{p_j}^{(t)}}$ that would reduce the total visits to p_j at time t down to the allowed maximum βM_{pj}, and then scale down all visits from each CBG c_i to p_j proportionately. For both reopening strategies, we calculate the predicted increase in cumulative incidence at the end of the reopening period (May 31, 2020), compared to the start of the reopening period (May 1, 2020).

Relative risk of reopening different categories of POIs (Figures 2d, Extended Data 5, S11, S15–S24). We study separately reopening the 20 POI categories with the most visits in SafeGraph data. In this analysis, we follow prior work[28] and do not study four categories: "Child Day Care Services" and "Elementary and Secondary Schools" (because children under 13 are not well-tracked by SafeGraph); "Drinking Places (Alcoholic Beverages)" (because SafeGraph seems to undercount these locations[28]) and "Nature Parks and Other Similar Institutions" (because boundaries and therefore areas are not well-defined by SafeGraph). We also exclude "General Medical and Surgical Hospitals" and "Other Airport Operations" (because hospitals and air travel both involve many additional risk factors our model is not designed to capture). We do not filter out these POIs during model fitting (i.e., we assume that people visit these POIs, and that transmissions occur there) because including them still increases the proportion of overall mobility our dataset captures; we simply do not analyze these categories, because we wish to be conservative and only focus on categories where we are most confident that we are capturing transmission faithfully.

This reopening analysis is similar to the previous experiments on reducing maximum occupancy vs. uniform reopening. As above, we set the reopening time τ to May 1, 2020, 12 AM. To simulate reopening a POI category, we take the set of POIs in that category, $\mathcal{V}$, and set their activity levels after reopening to that of the first week of March. For POIs not in the category $\mathcal{V}$, we keep their activity levels after reopening the same, i.e., we simply repeat the activity levels of the last week of our data (April 27–May 2, 2020): This gives us the visit matrix $\widetilde{W}^{(t)}$ with entries

$$\tilde{w}_{ij}^{(t)} := \begin{cases} w_{ij}^{(t)} & \text{if } t < \tau, \\ w_{ij}^{f(t)} & \text{if } t \geq \tau, p_j \in \mathcal{V} \\ w_{ij}^{g(t)} & \text{if } t \geq \tau, p_j \notin \mathcal{V}. \end{cases} \quad (31)$$

As in the above reopening analysis, $f(t)$ maps t to the corresponding hour in the first week of March, and $g(t)$ maps t to the corresponding hour in the last week of our data. For each category, we calculate the predicted difference between (1) the cumulative fraction of people who have been infected by the end of the reopening period (May 31, 2020) and (2) the cumulative fraction of people infected by May 31 had we not reopened the POI category (i.e., if we simply repeated the activity levels of the last week of our data). This seeks to model the increase in cumulative incidence by end of May from reopening the POI category. In Extended Data Figure 5 and Figures S15–S24, the bottom right panel shows the predicted increase for the category as a whole, and the bottom left panel shows the predicted increase *per POI* (i.e., the total increase divided by the number of POIs in the category).

Per-capita mobility (Figures 3d, Extended Data 6, S3). Each group of CBGs (e.g., the bottom income decile) comprises a set $\mathcal{U}$ of CBGs that fit the corresponding criteria. In Figure 3d and Extended Data Figure 6, we show the daily per-capita mobilities of different pairs of groups (broken down by income and by race). To measure the per-capita mobility of a group on day d, we take the total number of visits made from those CBGs to any POI, $\sum_{c_i \in \mathcal{U}} \sum_{p_j \in \mathcal{P}} \sum_{t=24d}^{24d+23} w_{ij}^{(t)}$, and divide it by the total population of the CBGs in the group, $\sum_{c_i \in \mathcal{U}} N_{c_i}$. In Figure S3, we show the total number of visits made by each group to each POI category, accumulated over the entire data period (March 1–May 2, 2020) and then divided by the total population of the group.

Average predicted transmission rate of a POI category (Figure 3e, Extended Data Tables 3–4). We compute the predicted average hourly transmission rate experienced by a group of CBGs $\mathcal{U}$ at a POI category $\mathcal{V}$ as

$$\overline{\beta}_{\mathcal{U}\mathcal{V}} := \frac{\sum_{c_i \in \mathcal{U}} \sum_{p_j \in \mathcal{V}} \sum_{t=1}^{T} w_{ij}^{(t)} \beta_{p_j}^{(t)}}{\sum_{c_i \in \mathcal{U}} \sum_{p_j \in \mathcal{V}} \sum_{t=1}^{T} w_{ij}^{(t)}}, \quad (32)$$

where, as above, $\beta_{p_j}^{(t)}$ is the transmission rate at POI p_j in hour t (Equation (8)), $w_{ij}^{(t)}$ is the number of visitors from CBG c_i at POI p_j in hour t, and T is the last hour in our simulation. This represents the expected transmission rate encountered during a visit by someone from a CBG in group $\mathcal{U}$ to a POI in category $\mathcal{V}$.

Reporting summary

Further information on research design is available in the Nature Research Reporting Summary linked to this paper.

Data availability

Inferred hourly mobility networks as well as the estimated models are available at the project website http://covid-mobility.stanford.edu. Raw census data (https://www.census.gov/programs-surveys/acs), case and death counts from *The New York Times* (https://github.com/nytimes/covid-19-data), and Google mobility data (https://www.google.com/covid19/mobility/) are also publicly available. Cell phone mobility data is freely available to researchers, non-profits, and governments through the SafeGraph COVID-19 Data Consortium (https://www.safegraph.com/covid-19-data-consortium).

Code availability

Code is publicly available at the project website http://covid-mobility.stanford.edu.

39. SafeGraph. Places Schema (2020). Available at https://docs.safegraph.com/docs/places-schema.
40. SafeGraph. Weekly Patterns (2020). Available at https://docs.safegraph.com/docs/weekly-patterns.
41. SafeGraph. Using SafeGraph Polygons to Estimate Point-Of-Interest Square Footage (2019). Available at https://www.safegraph.com/blog/using-safegraph-polygons-to-estimate-point-of-interest-square-footage.
42. SafeGraph. Guide to Points-of-Interest Data: POI Data FAQ (2020). Available at https://www.safegraph.com/points-of-interest-poi-data-guide.
43. SafeGraph. Social Distancing Metrics (2020). Available at https://docs.safegraph.com/docs/social-distancing-metrics.
44. Athey, S. & *et al*. Estimating heterogeneous consumer preferences for restaurants and travel time using mobile location data. In *AEA Papers and Proceedings* **108**, 64–67 (2018).
45. Chen, M. K. & Rohla, R. The effect of partisanship and political advertising on close family ties. *Science* **360**, 1020–1024 (2018).
46. Farboodi, M., Jarosch, G. & Shimer, R. Internal and external effects of social distancing in a pandemic (2020). Available at https://nber.org/papers/w27059.
47. Killeen, B. D. & *et al*. A County-level Dataset for Informing the United States' Response to COVID-19 (2020). Available at https://arxiv.org/abs/2004.00756.
48. Allcott, H. & *et al*. Polarization and public health: Partisan differences in social distancing during the Coronavirus pandemic (2020). Available at nber.org/papers/w26946.
49. Google. COVID-19 Community Mobility Reports (2020). Available at https://google.com/covid19/mobility/.
50. Athey, S. & *et al*. Experienced Segregation (2019). Available at https://gsb.stanford.edu/faculty-research/working-papers/experienced-segregation.
51. Squire, R. F. What about bias in the SafeGraph dataset? (2019). Available at https://safegraph.com/blog/what-about-bias-in-the-safegraph-dataset.
52. US Census. American Community Survey. Available at https://census.gov/programs-surveys/acs.
53. Bishop, Y. M., Fienberg, S. E. & Holland, P. W. Discrete multivariate analysis (1975).
54. Birkin, M. & Clarke, M. SYNTHESIS—a synthetic spatial information system for urban and regional analysis: methods and examples. *Environment and planning A* **20**, 1645–1671 (1988).
55. Wong, D. W. The reliability of using the iterative proportional fitting procedure. *The Professional Geographer* **44**, 340–348 (1992).

56. Simpson, L. & Tranmer, M. The reliability of using the iterative proportional fitting procedure. *The Professional Geographer* **57**, 222–234 (2005).
57. Hu, H., Nigmatulina, K. & Eckhoff, P. The scaling of contact rates with population density for the infectious disease models. *Mathematical Biosciences* **244**, 125–134 (2013).
58. Kucharski, A. J. *et al*. Early dynamics of transmission and control of COVID-19: a mathematical modelling study. *The Lancet Infectious Diseases* **20**, 553 – 558 (2020).
59. Park, M. *et al*. A systematic review of COVID-19 epidemiology based on current evidence. *Journal of Clinical Medicine* **9**, 967 (2020).
60. Curmei, M. *et al*. Estimating Household Transmission of SARS-CoV-2. *medRxiv* (2020). Available at https://doi.org/10.1101/2020.05.23.20111559.
61. Li, W. *et al*. The characteristics of household transmission of COVID-19. *Clinical Infectious Diseases* (2020).
62. Gudbjartsson, D. F. *et al*. Spread of SARS-CoV-2 in the Icelandic population. *New England Journal of Medicine* **382**, 2302–2315 (2020).
63. Carey, B. & Glanz, J. Hidden Outbreaks Spread Through U.S. Cities Far Earlier Than Americans Knew, Estimates Say. *The New York Times* (2020). Available at https://nytimes.com/2020/04/23/us/coronavirus-early-outbreaks-cities.html.
64. Bommer, C. & Vollmer, S. Average detection rate of SARS-CoV-2 infections has improved since our last estimates but is still as low as nine percent on March 30th (2020). Available at https://www.uni-goettingen.de/en/606540.html.
65. Javan, E., Fox, S. J., & Meyers, L. A. The unseen and pervasive threat of COVID-19 throughout the US. *medRxiv* (2020). Available at https://doi.org/10.1101/2020.04.06.20053561.
66. Perkins, T. A. *et al*. Estimating unobserved SARS-CoV-2 infections in the United States. *Proceedings of the National Academy of Sciences* **117**, 22597–22602 (2020).
67. King, A. A. *et al*. Avoidable errors in the modelling of outbreaks of emerging pathogens, with special reference to Ebola. *Proceedings of the Royal Society B: Biological Sciences* **282**, 20150347 (2015).

Acknowledgements The authors thank Yong-Yeol Ahn, Ruth Appel, Caroline Chen, Jean Feng, Nic Fishman, Scott Fullerton, Tatsunori Hashimoto, Percy Liang, Kyle Loh, Derek Ouyang, Roni Rosenfeld, Shiori Sagawa, Jacob Steinhardt, Ryan Tibshirani, Johan Ugander, Damir Vrabac, seminar participants, and our reviewers for support and helpful comments. We also thank Nick Singh, Ryan Fox Squire, Jessica Williams-Holt, Jonathan Wolf, Ruowei Yang, and others at SafeGraph for cell phone mobility data and helpful feedback. This research was supported by US National Science Foundation under OAC-1835598 (CINES), OAC-1934578 (HDR), CCF-1918940 (Expeditions), IIS-2030477 (RAPID), Stanford Data Science Initiative, Wu Tsai Neurosciences Institute, and Chan Zuckerberg Biohub. S.C. was supported by an NSF Fellowship. E.P. was supported by a Hertz Fellowship. P.W.K. was supported by the Facebook Fellowship Program. J.L. is a Chan Zuckerberg Biohub investigator.

Author contributions S.C., E.P., and P.W.K. performed computational analysis. All authors jointly analyzed the results and wrote the paper.

Competing interests The authors declare no competing interests.

Additional information

Supplementary information is available for this paper at https://doi.org/10.1038/s41586-020-2923-3.

Correspondence and requests for materials should be addressed to J.L.

Peer review information *Nature* thanks Moritz Kraemer, Marc Lipsitch and the other, anonymous, reviewer(s) for their contribution to the peer review of this work. Peer reviewer reports are available.

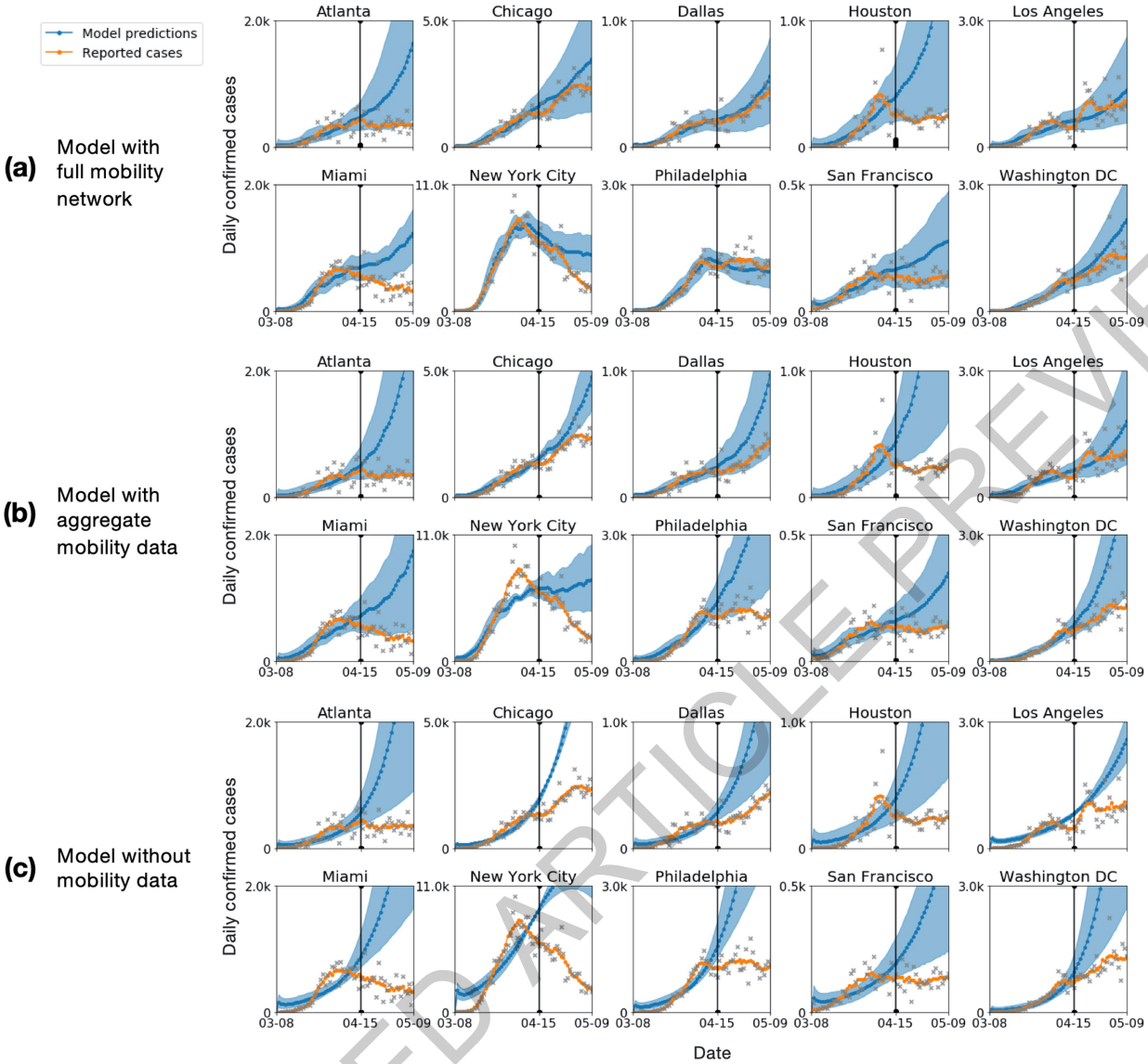

Extended Data Figure 1 | Mobility-based epidemiological model and its predictions. Predicted (blue) and true (orange) daily case counts for **(a)** our model, which uses hourly mobility networks, **(b)** an SEIR model which uses hourly aggregated mobility data, and **(c)** a baseline SEIR model which does not use mobility data (see Methods M3.4 for details). Incorporating mobility information improves out-of-sample fit and having a network, instead of an aggregate measure, further improves fit: on average across metro areas, our best-fit network model's out-of-sample error (RMSE) was only 58% that of the best-fit aggregate mobility model. All three models are calibrated on observed case counts before April 15, 2020 (vertical black line). The grey x's represent the daily reported cases; since they tend to have great variability, we also show the smoothed weekly average (orange line). Shaded regions denote 2.5th and 97.5th percentiles across sampled parameters and stochastic realizations.

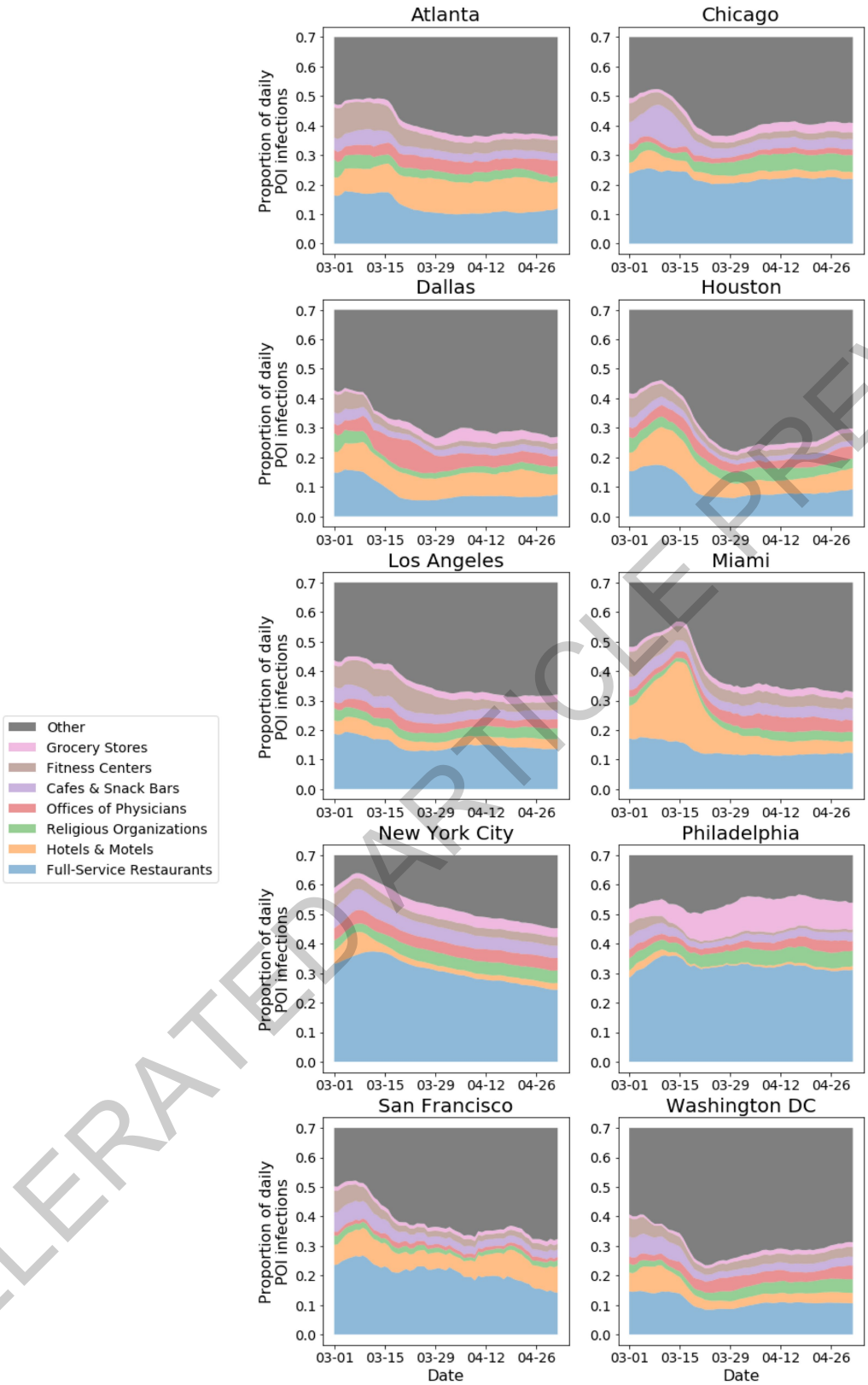

Extended Data Figure 2 | Distribution of POI infections over time. We selected the POI categories that our models predicted contributed the most to infections, and plotted the predicted *proportion* of POI infections each category accounted for over time. Our model predicts time-dependent variation of where transmissions may have occurred. For example, Full-Service Restaurants (blue) and Fitness Centers (brown) contributed less to predicted infections over time, likely due to lockdown orders closing these POIs, while grocery stores remained steady or even grew in their predicted contribution, likely because they remained open as essential businesses. Hotels & Motels (yellow) also feature in these plots; most notably, the model predicts a peak in their contributed infections in Miami around mid-March – this would align with college spring break, with Miami as a popular vacation spot for students. The proportions are stacked in these plots, and the y-axes are truncated at 0.7 because every plot would only show "Other" from 0.7 to 1.0.

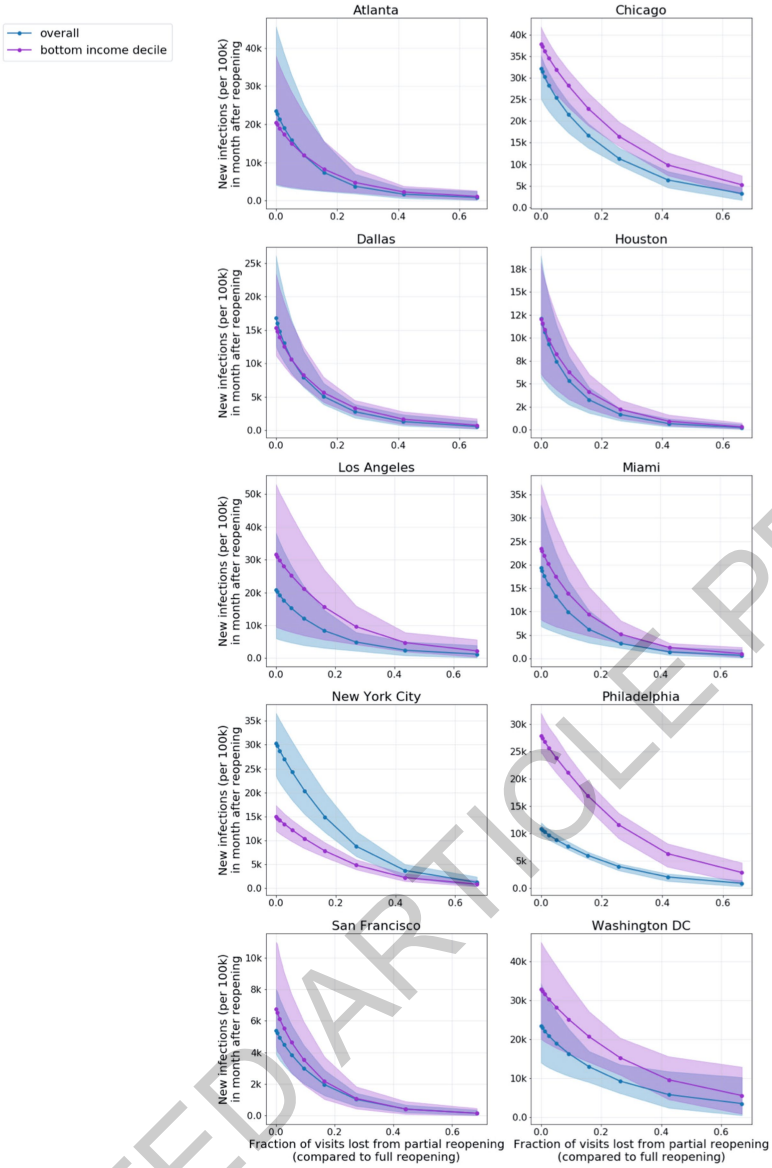

Extended Data Figure 3 | Trade-off between new infections and visits lost from reopening. We simulate reduced maximum occupancy reopening starting on May 1, 2020 and run the simulation until the end of the month. Each dot represents the level of occupancy reduction : e.g., capping visits at 50% of maximum occupancy. The y-coordinate represents the predicted number of new infections incurred after reopening (per 100k population) and the x-coordinate represents the fraction of visits lost from partial reopening compared to full reopening. Shaded regions denote 2.5th and 97.5th percentiles across parameter sets and stochastic realizations. In 4 metro areas, the predicted cost of new infections from reopening is roughly similar for lower-income CBGs and the overall population, but in 5 metro area s, the lower-income CBGs incur more predicted infections from reopening. Notably, New York City (NYC) is the only metro area where this trend is reversed; this is because the model predicts that such a high fraction—65% (95% CI, 62%–68%) – of lower-income CBGs in NYC had been infected before reopening that after reopening, only a minority of the lower-income population is still susceptible (in comparison, the second highest fraction infected before reopening was 31% (95% CI, 28%–35%) for Philadelphia, and the rest ranged from 1%–14%).

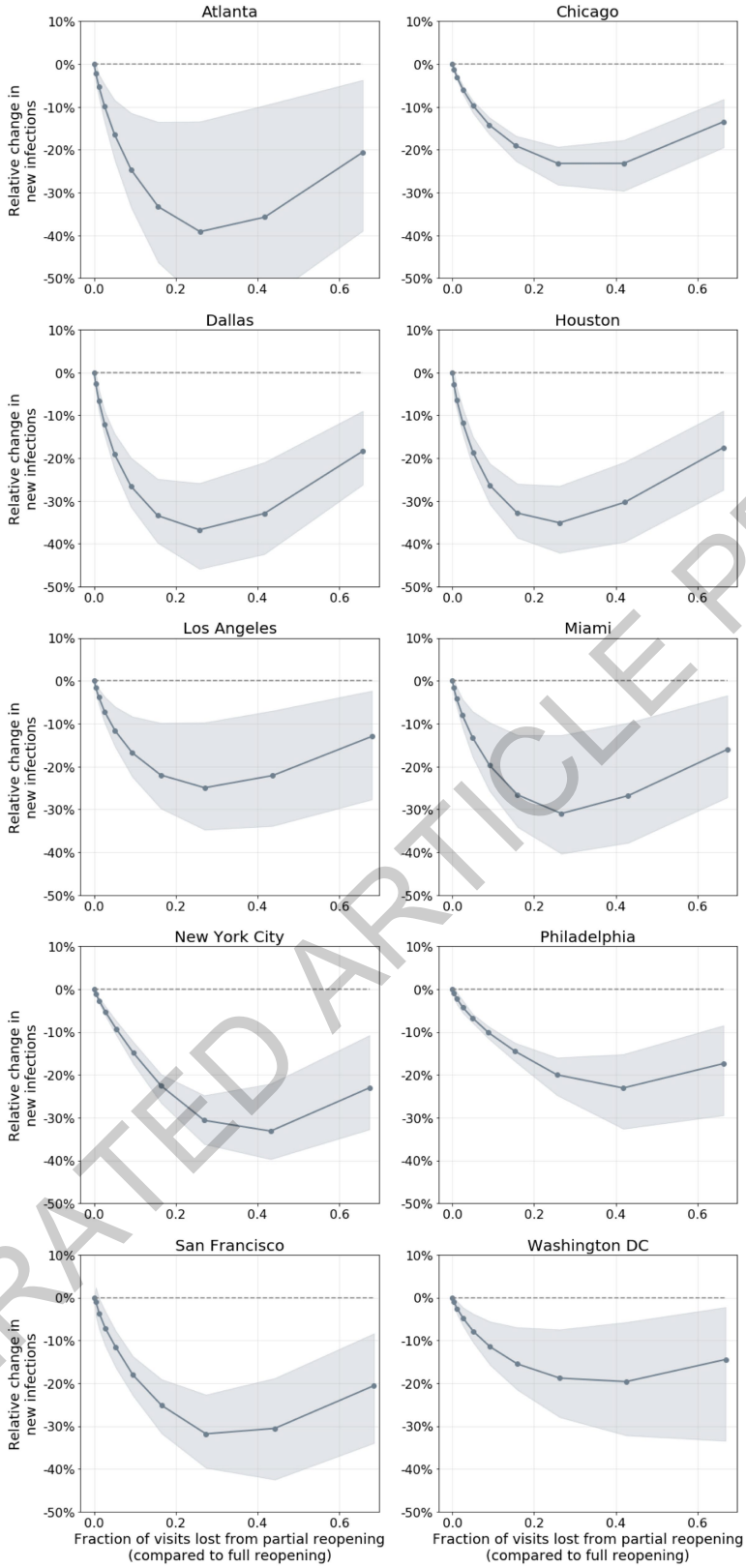

Extended Data Figure 4 | Reduced maximum occupancy versus uniform reduction reopening. Compared to partially reopening by uniformly reducing visits, the reduced maximum occupancy strategy—which disproportionately targets high-risk POIs with sustained high occupancy—always results in a smaller predicted increase in infections for the same number of visits. The y-axis plots the relative difference between the predicted increase in cumulative infections (from May 1 to May 31) under the reduced occupancy strategy as compared to the uniform reduction strategy. The shaded regions denote the 2.5th and 97.5th percentiles over sampled parameters and stochastic realizations.

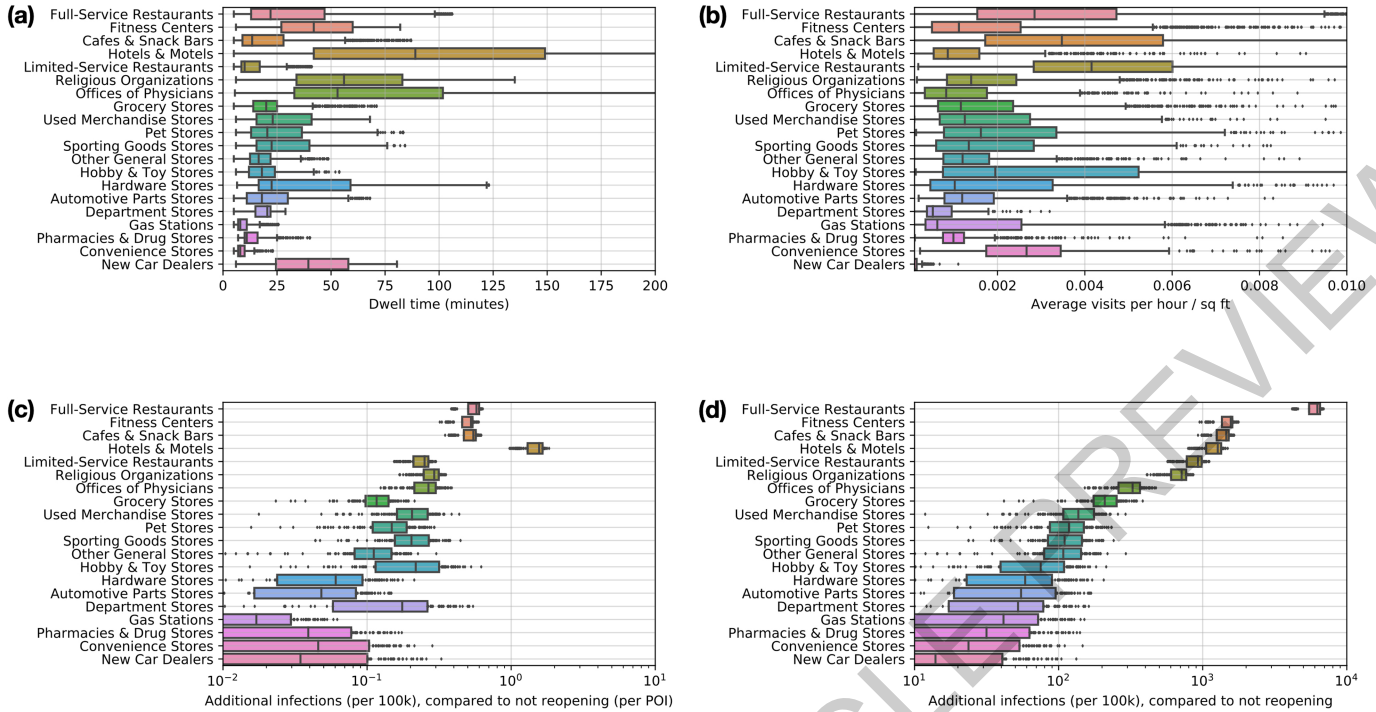

Extended Data Figure 5 | POI attributes in all 10 metro area s combined. The top two plots pool POIs from all metro area s and plot quantities from the mobility data, showing **(a)** the distribution of dwell time, and **(b)** the average number of hourly visitors divided by the area of the POI in square feet. Each point represents one POI; boxes depict the interquartile range across POIs, with data points outside the range individually shown. The bottom two plots pool across model realizations from all metro area s, and show model predictions for the increase in infections (per 100k population) from reopening a POI category: **(c)** per POI, and **(d)** for the category as a whole. Each point represents a model realization; boxes depict the interquartile range across realizations, with data points outside the range individually shown. Across MSAs, we model 552,758 POIS in total, and we sample 97 parameters and 30 stochastic realizations (N = 2,910); see Table S6 for the number of sets per metro area. The boxes denote the interquartile range, with data points outside the range individually shown. Colors are used to distinguish the different POI categories, but do not have any additional meaning.

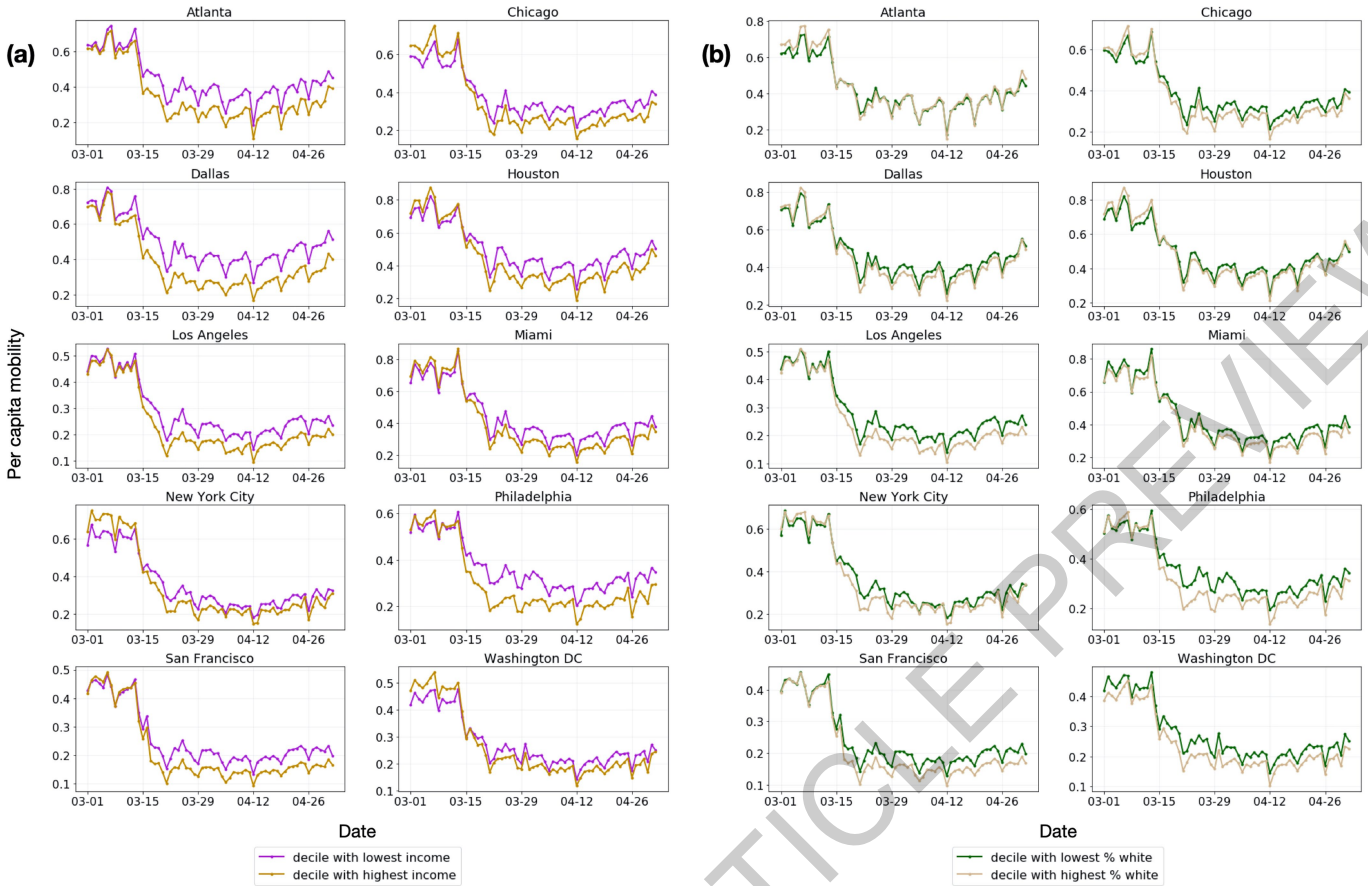

Extended Data Figure 6 | Daily per-capita mobility over time. We compare mobility in the lowest/highest deciles of CBGs based on **(a)** median household income and **(b)** percentage of white residents. See Methods M5 for details.

Extended Data Table 1 | Dataset summary statistics from March 1–May 2, 2020

Metro area	CBGs	POIs	Hourly edges	Total modeled pop	Total visits
Atlanta	3,130	39,411	540,166,727	7,455,619	27,669,692
Chicago	6,812	62,420	540,112,026	10,169,539	33,785,702
Dallas	4,877	52,999	752,998,455	9,353,561	37,298,053
Houston	3,345	49,622	609,766,288	7,621,541	32,943,613
Los Angeles	8,904	83,954	643,758,979	16,101,274	38,101,674
Miami	3,555	40,964	487,544,190	6,833,129	26,347,947
New York City	14,763	122,428	1,057,789,207	20,729,481	66,581,080
Philadelphia	4,565	37,951	304,697,220	6,759,058	19,551,138
San Francisco	2,943	28,713	161,575,167	5,137,800	10,728,090
Washington DC	4,051	34,296	312,620,619	7,740,276	17,898,324
All metro areas combined	**56,945**	**552,758**	**5,411,028,878**	**97,901,278**	**310,905,313**

Extended Data Table 2 | Model parameters

Param.	Description	Value (Source)
δ_E	mean latency period	96 hours[24,63]
δ_I	mean infectious period	84 hours[24]
δ_c	period from infectious to confirmed	7 days[24,71]
r_c	percentage of cases which are detected	10%[24,63,69–71]
β_{base}	base CBG transmission rate	Variable (Estimated)
N_{c_i}	population size of CBG c_i	Variable (2018 US Census[57])
ψ	scaling factor for POI transmission	Variable (Estimated)
$w_{ij}^{(t)}$	# visitors from CBG c_i to POI p_j at time t	Variable (SafeGraph)
a_{p_j}	area of POI p_j in square feet	Variable (SafeGraph)
p_0	initial proportion of exposed population	Variable (Estimated)
$S_{c_i}^{(0)}$	initial susceptible population in CBG c_i	$(1-p_0)N_{c_i}$
$E_{c_i}^{(0)}$	initial exposed population in CBG c_i	$p_0 N_{c_i}$
$I_{c_i}^{(0)}$	initial infectious population in CBG c_i	0
$R_{c_i}^{(0)}$	initial removed population in CBG c_i	0

If the parameter has a fixed value, we specify it under **Value**; otherwise, we write "Variable" to indicate that it varies across CBG / POI / metro area.

Extended Data Table 3 | Predicted transmission rate disparities at each POI category between income groups

Metro area	ATL	CHI	DAL	HOU	LA	MIA	NY	PHL	SF	DC	**Median**
Full-Service Restaurants	0.764	1.204	0.956	1.000	1.445	1.232	2.035	2.883	1.758	1.171	1.218
Limited-Service Restaurants	0.940	0.950	1.002	0.906	1.067	0.872	1.901	1.614	0.994	0.962	0.978
Other General Stores	0.782	1.083	0.957	0.729	0.760	0.894	1.218	1.312	1.045	0.950	0.954
Gas Stations	1.326	1.865	1.310	1.515	2.254	2.195	1.899	6.461	1.357	1.870	1.868
Fitness Centers	0.536	0.907	0.708	0.670	1.461	0.789	1.151	1.516	0.995	1.160	0.951
Grocery Stores	0.948	3.080	0.838	1.333	2.408	1.498	4.984	10.437	2.478	1.977	2.192
Cafes & Snack Bars	1.385	0.919	0.716	1.120	1.327	2.168	1.943	1.757	0.982	0.932	1.224
Hotels & Motels	1.228	1.200	0.814	0.804	1.229	1.134	1.260	1.993	1.199	1.346	1.214
Religious Organizations	1.546	1.763	0.956	0.919	1.746	1.464	1.756	1.736	1.515	1.852	1.641
Hardware Stores	3.938	3.340	1.575	2.111	1.333	0.939	3.553	6.716	4.202	13.560	3.446
Department Stores	1.132	1.230	0.978	0.911	1.083	1.431	1.667	0.976	0.867	1.042	1.062
Offices of Physicians	1.235	0.721	0.667	1.036	1.141	1.687	1.307	1.319	1.193	0.445	1.167
Pharmacies & Drug Stores	1.636	1.389	1.176	0.854	1.718	1.555	2.577	5.624	1.200	1.699	1.596
Sporting Goods Stores	0.936	1.540	1.129	0.812	1.168	0.700	1.253	1.161	0.826	2.777	1.145
Automotive Parts Stores	0.890	1.707	0.862	1.086	1.990	1.414	1.524	2.697	1.753	1.246	1.469
Used Merchandise Stores	0.993	0.931	1.000	1.315	1.017	1.074	1.352	1.668	1.587	0.814	1.046
Convenience Stores	1.208	0.932	1.613	0.647	0.838	0.824	1.736	2.322	1.086	1.428	1.147
Pet Stores	1.260	0.820	1.192	1.487	1.536	0.776	3.558	1.652	2.124	0.905	1.374
New Car Dealers	2.036	1.471	0.741	0.809	1.180	1.377	2.022	1.129	0.395	0.872	1.154
Hobby & Toy Stores	1.168	1.110	1.165	0.853	1.771	1.520	1.525	1.088	0.883	0.926	1.138
Median	1.188	1.202	0.968	0.915	1.330	1.305	1.746	1.702	1.196	1.166	

We report the ratio of the average predicted transmission rate encountered by visitors from CBGs in the bottom income decile to that for the top income decile. A ratio greater than 1 means that visitors from CBGs in the bottom income decile experienced higher (more dangerous) predicted transmission rates. See Methods M5 for details.

Extended Data Table 4 | Predicted transmission rate disparities at each POI category between racial groups

Metro area	ATL	CHI	DAL	HOU	LA	MIA	NY	PHL	SF	DC	**Median**
Full-Service Restaurants	0.802	1.354	0.981	0.965	1.065	1.167	2.418	2.661	1.223	1.013	1.116
Limited-Service Restaurants	0.940	1.144	1.028	0.940	0.820	0.919	2.136	1.523	0.799	1.346	0.984
Other General Stores	0.776	1.277	0.838	0.841	1.527	1.132	2.158	1.313	0.925	1.312	1.204
Gas Stations	1.402	1.891	1.389	1.190	1.336	1.857	1.818	2.286	2.321	1.316	1.610
Fitness Centers	0.607	1.167	0.670	0.831	0.780	1.066	1.447	1.977	1.103	1.205	1.084
Grocery Stores	0.589	3.664	0.613	1.195	2.386	0.950	5.864	13.705	2.243	2.262	2.252
Cafes & Snack Bars	1.308	1.104	0.845	0.840	0.976	2.619	1.767	2.456	1.045	0.867	1.074
Hotels & Motels	0.977	1.007	1.366	0.718	1.112	1.024	1.449	2.494	0.654	0.899	1.015
Religious Organizations	0.938	1.606	1.060	0.953	2.096	1.795	1.933	2.040	1.674	1.188	1.640
Hardware Stores	0.909	3.900	1.523	1.461	1.952	0.586	5.032	3.898	11.103	13.432	2.925
Department Stores	1.081	1.301	0.805	0.777	0.992	2.337	2.479	1.357	1.089	1.402	1.195
Offices of Physicians	0.894	1.323	1.006	1.415	0.898	1.117	1.652	2.073	0.694	1.911	1.220
Pharmacies & Drug Stores	0.888	1.376	0.930	0.732	1.538	1.674	3.315	3.366	1.135	1.715	1.457
Sporting Goods Stores	0.767	0.674	0.650	0.506	1.946	0.818	1.532	2.152	0.880	1.715	0.849
Automotive Parts Stores	1.049	1.479	1.010	1.353	2.998	2.657	1.740	3.387	1.646	0.601	1.562
Used Merchandise Stores	0.858	1.195	0.699	1.060	1.270	0.593	1.500	3.024	1.425	0.799	1.128
Convenience Stores	2.016	5.055	1.272	2.188	0.761	0.902	1.911	2.276	1.239	1.844	1.878
Pet Stores	0.925	1.624	0.724	1.465	1.506	0.881	2.715	10.182	1.568	2.408	1.537
New Car Dealers	1.008	1.398	0.812	0.736	0.942	0.998	1.977	0.866	0.772	0.383	0.904
Hobby & Toy Stores	2.569	0.853	0.628	0.979	1.373	1.388	2.237	0.825	0.864	1.286	1.132
Median	0.932	1.339	0.888	0.959	1.303	1.092	1.955	2.281	1.119	1.314	

We report the ratio of the average predicted transmission rate encountered by visitors from CBGs with the lowest (bottom decile) proportion of white residents versus that for the top decile. A ratio greater than 1 means that visitors from CBGs in the bottom decile experienced higher (more dangerous) predicted transmission rates. See Methods M5 for details.

nature research

Corresponding author(s): Jure Leskovec

Last updated by author(s): Oct 7, 2020

Reporting Summary

Nature Research wishes to improve the reproducibility of the work that we publish. This form provides structure for consistency and transparency in reporting. For further information on Nature Research policies, see our Editorial Policies and the Editorial Policy Checklist.

Statistics

For all statistical analyses, confirm that the following items are present in the figure legend, table legend, main text, or Methods section.

n/a	Confirmed	
☐	☒	The exact sample size (*n*) for each experimental group/condition, given as a discrete number and unit of measurement
☐	☒	A statement on whether measurements were taken from distinct samples or whether the same sample was measured repeatedly
☐	☒	The statistical test(s) used AND whether they are one- or two-sided *Only common tests should be described solely by name; describe more complex techniques in the Methods section.*
☐	☒	A description of all covariates tested
☐	☒	A description of any assumptions or corrections, such as tests of normality and adjustment for multiple comparisons
☐	☒	A full description of the statistical parameters including central tendency (e.g. means) or other basic estimates (e.g. regression coefficient) AND variation (e.g. standard deviation) or associated estimates of uncertainty (e.g. confidence intervals)
☒	☐	For null hypothesis testing, the test statistic (e.g. *F*, *t*, *r*) with confidence intervals, effect sizes, degrees of freedom and *P* value noted *Give P values as exact values whenever suitable.*
☒	☐	For Bayesian analysis, information on the choice of priors and Markov chain Monte Carlo settings
☒	☐	For hierarchical and complex designs, identification of the appropriate level for tests and full reporting of outcomes
☐	☒	Estimates of effect sizes (e.g. Cohen's *d*, Pearson's *r*), indicating how they were calculated

Our web collection on statistics for biologists contains articles on many of the points above.

Software and code

Policy information about availability of computer code

Data collection	No data collection was performed for this study; all analysis relied on previously collected datasets, as described in the Data section below.
Data analysis	All data analysis was performed using Python with standard libraries. Code is available at http://snap.stanford.edu/covid-mobility and https://github.com/snap-stanford/covid-mobility.

For manuscripts utilizing custom algorithms or software that are central to the research but not yet described in published literature, software must be made available to editors and reviewers. We strongly encourage code deposition in a community repository (e.g. GitHub). See the Nature Research guidelines for submitting code & software for further information.

Data

Policy information about availability of data

All manuscripts must include a data availability statement. This statement should provide the following information, where applicable:

- Accession codes, unique identifiers, or web links for publicly available datasets
- A list of figures that have associated raw data
- A description of any restrictions on data availability

Census data (https://www.census.gov/programs-surveys/acs), case and death counts from The New York Times (https://github.com/nytimes/covid-19-data), and Google mobility data (https://www.google.com/covid19/mobility/) are publicly available. Cell phone mobility data is freely available to researchers, non-profits, and governments through the SafeGraph COVID-19 Data Consortium (https://www.safegraph.com/covid-19-data-consortium).

Field-specific reporting

Please select the one below that is the best fit for your research. If you are not sure, read the appropriate sections before making your selection.

☐ Life sciences ☒ Behavioural & social sciences ☐ Ecological, evolutionary & environmental sciences

For a reference copy of the document with all sections, see nature.com/documents/nr-reporting-summary-flat.pdf

Behavioural & social sciences study design

All studies must disclose on these points even when the disclosure is negative.

Study description	This is a quantitative epidemiological modeling study.
Research sample	We study previously-collected data on 10 of the largest American metropolitan statistical areas. The data came from the following: 1) Anonymized mobility data from smartphone users from SafeGraph. SafeGraph data is obtained by "partnering with mobile applications that obtain opt-in consent from its users to collect anonymous location data", per official SafeGraph documentation. 2) US Census 3) Case and death counts from The New York Times 4) Google mobility data
Sampling strategy	We did not perform sampling, but relied on previously collected datasets. All datasets were chosen as they were comprehensive: the case and death counts and Census data were designed to cover the entire population; Google mobility data covers a large subset of the population; and previous analyses have shown that the SafeGraph anonymized cell phone mobility dataset is geographically representative: for example, it does not systematically over-represent individuals from higher-income areas (https://www.safegraph.com/blog/what-about-bias-in-the-safegraph-dataset).
Data collection	We did not perform data collection, but relied on previously collected datasets. Census data is collected as described here: https://www.census.gov/programs-surveys/acs. The cell phone mobility data is collected from cell phone geolocation information, and is anonymized and aggregated. We accessed and downloaded the datasets in May 2020.
Timing	We make use of data in the following ranges: 1) Safegraph mobility data: Jan 1, 2019 - May 2, 2020 2) US Census: 2013-2018 3) Case and death counts from The New York Times: March 8 - May 9, 2020 4) Google mobility data: March 1 - May 2, 2020
Data exclusions	The original SafeGraph dataset contains 5.4 million points of interest (POIs). We retain a POI in our final dataset if it satisfies the following criteria: (1) it lies within one of the 10 American metropolitan areas that we analyze (out of 384 metropolitan statistical areas total); (2) SafeGraph has visit data for this POI for every hour that we model, from 12am on March 1, 2020 to 11pm on May 2, 2020; (3) SafeGraph has recorded the home CBGs of this POI's visitors for at least one month from January 2019 to February 2020; (4) the POI is not a "parent" POI, as defined in the Methods section. After applying these filters, our dataset contains 553k POIs. Most POIs are filtered out because they do not lie within the 10 large metropolitan statistical areas that we study; this filtering decision was made prior to any analysis for computational tractability reasons. In our analysis of POI-specific category risks, we do not analyze 6 categories of POIs because we wish to be conservative and only focus on categories where we are most confident we are fully capturing transmission at the category: Child Day Care Services, Elementary and Secondary Schools, Drinking Places (Alcoholic Beverages), Nature Parks and Other Similar Institutions, General Medical and Surgical Hospitals, and Other Airport Operations. The justifications for these exclusions, which are based on prior work, are given in the Methods section.
Non-participation	Because we relied on previously collected anonymized, aggregated data from cell phone mobility tracking, we did not have access to individual-level data and do not know how many participants dropped out/declined participation.
Randomization	This is not a randomized controlled trial and participants were not randomized into experimental groups.

Reporting for specific materials, systems and methods

We require information from authors about some types of materials, experimental systems and methods used in many studies. Here, indicate whether each material, system or method listed is relevant to your study. If you are not sure if a list item applies to your research, read the appropriate section before selecting a response.

Materials & experimental systems

n/a	Involved in the study
☒	☐ Antibodies
☒	☐ Eukaryotic cell lines
☒	☐ Palaeontology and archaeology
☒	☐ Animals and other organisms
☐	☒ Human research participants
☒	☐ Clinical data
☒	☐ Dual use research of concern

Methods

n/a	Involved in the study
☒	☐ ChIP-seq
☒	☐ Flow cytometry
☒	☐ MRI-based neuroimaging

Human research participants

Policy information about studies involving human research participants

Population characteristics	See above.
Recruitment	See above. Prior work has looked into biases in the SafeGraph dataset (https://www.safegraph.com/blog/what-about-bias-in-the-safegraph-dataset).
Ethics oversight	The dataset from The New York Times consists of aggregated COVID-19 confirmed case and death counts collected by journalists from public news conferences and public data releases. For the mobility data, consent was obtained by the third-party sources collecting the data. SafeGraph aggregates data from mobile applications that obtain opt-in consent from their users to collect anonymous location data. Google's mobility data consists of aggregated, anonymized sets of data from users who have chosen to turn on the Location History setting. Additionally, we obtained IRB exemption for SafeGraph data from the Northwestern University IRB office.

Note that full information on the approval of the study protocol must also be provided in the manuscript.